

**A STUDY OF MARINE CARBONATE MOUNDS OFF BAY ST.
LAWRENCE, CAPE BRETON ISLAND, NOVA SCOTIA**

Matthew Donald Harrington

Submitted in Partial Fulfillment of the Requirements for the
Degree of Bachelor of Science, Combined Honours
Department of Earth Sciences
Dalhousie University, Halifax, Nova Scotia
March 20, 2003



Dalhousie University

Department of Earth Sciences

Halifax, Nova Scotia

Canada B3H 3J5

(902) 494-2358

FAX (902) 494-6889

DATE April 30/03

AUTHOR Matthew Harrington

TITLE A Study of Marine Carbonate Mounds
off Bay St. Lawrence, Cape Breton Island,
Nova Scotia

Degree _____ Convocation _____ Year _____

Permission is herewith granted to Dalhousie University to circulate and to have copied for non-commercial purposes, at its discretion, the above title upon the request of individuals or institutions.

THE AUTHOR RESERVES OTHER PUBLICATION RIGHTS, AND NEITHER THE THESIS NOR EXTENSIVE EXTRACTS FROM IT MAY BE PRINTED OR OTHERWISE REPRODUCED WITHOUT THE AUTHOR'S WRITTEN PERMISSION.

THE AUTHOR ATTESTS THAT PERMISSION HAS BEEN OBTAINED FOR THE USE OF ANY COPYRIGHTED MATERIAL APPEARING IN THIS THESIS (OTHER THAN BRIEF EXCERPTS REQUIRING ONLY PROPER ACKNOWLEDGEMENT IN SCHOLARLY WRITING) AND THAT ALL SUCH USE IS CLEARLY ACKNOWLEDGED.

Abstract

Marine carbonate mud mounds occur 5km northwest of Bay St. Lawrence, Cape Breton Island, on a 160 – 210m ridge before the upper margin of the Laurentian Channel. The marine carbonate mounds occur subsurface of the Holocene siliciclastic sediments and are thought to be a recent formation. Samples from these < 1m high mounds are of three textural varieties: (1) knobby popcorn-clustered, (2) muddy, (3) and erosional. All varieties are highly porous with numerous small pore holes (<3mm). Internally, the mounds are a low-Mg muddy micrite with no lamination. Concentrically banded acicular and radial sparite occurs in pore spaces. They have comparable characteristics with many cold-water and marine carbonate formations, but the absence of an abundant biological component and the uncommon internal structure make these marine carbonate mounds unique. Formation of the marine carbonate mounds may originate from hydrocarbon fluid seepage, seawater geochemistry at the sediment interface, the circulation of various pore waters, or the biological activity of various marine biotas.

Table of Contents

Table of Contents	ii
Table of Figures	iv
Table of Tables	v
Acknowledgements	vi
Chapter 1: Introduction	
1.1 Introduction	1
1.2 Purpose	1
1.3 Location and Distribution	2
1.4 Surficial Geology and Geomorphology	2
1.5 Scope	4
1.6 Organization	5
Chapter 2: Background	
2.1 Introduction	6
2.2 Carbonate Classification	6
2.3 Porosity	7
2.4 Carbonate Mud Mounds	9
2.5 Concretions	11
2.6 Cold-seeps and Carbonate Formation	12
2.7 Submarine Hardgrounds	13
2.8 Speleothems	13
Chapter 3: Methodology	
3.1 Sample Collection	14
3.2 Macroscopic Analysis	14
3.3 Petrographic Analysis	14
3.4 Carbonate Percentage Determination	15
3.5 Microprobe Analysis	15
3.6 Hydrocarbon Detection	15
Chapter 4: Results	
4.1 Structures and Textures	16
4.1.1 Introduction	16
4.1.2 Sample A1 - Popcorn	18
4.1.3 Sample A2 - Muddy	20
4.1.4 Sample A3 - Popcorn	22
4.1.5 Sample A4 - Erosional	24
4.1.6 Sample A5 - Erosional	24
4.1.7 Sample A6 - Muddy	27

4.2 Carbonate Percentage	27
4.3 Internal Structures	29
4.3.1 Distribution	31
4.3.2 Lime Mud	31
4.3.3 Popcorn Structures	32
4.3.4 Sparite and Polymictic Conglomerate	32
4.3.5 Small Pores	34
4.4 Petrography	34
4.4.1 Micrite	34
4.4.2 Sparite	36
4.5 Microprobe Analysis	40
 Chapter 5: Discussion	
5.1: Introduction	42
5.2: Layering and Concretionary Formation	42
5.3: Crystal Morphology and Mineralogy	43
5.4: Lime Mud Neomorphism (Diagenesis)	44
5.5: Polymictic Conglomerate	45
5.6: Popcorn Structures	46
5.7: Erosion	47
5.8: Origin	47
5.9: Timing	49
 Chapter 6: Conclusion	
6.1: Timing	51
6.2: Possible Origins	51
6.3: Classification	51
6.4: Future Work	51
References	53
Appendix A	55
Appendix B	59

Table of Figures

Figure 1.1	Glacial Stratigraphy of the Gulf of St. Lawrence	3
Figure 2.1	Mud mound classification	10
Figure 2.2	Concretion formation	11
Figure 4.1	The morphology of the six carbonate samples	17
Figure 4.2	Textural features of sample A1	19
Figure 4.3	Textural features of sample A2	21
Figure 4.4	Textural features of sample A3	23
Figure 4.5	Textural features of sample A4	25
Figure 4.6	Textural features of sample A5	26
Figure 4.7	Textural features of sample A6	28
Figure 4.8	Cross-sectional view of a carbonate specimen	30
Figure 4.9	Cross-sectional view of a polymictic conglomerate	33
Figure 4.10	Concentrically banded sparite	33
Figure 4.11	Cross-sectional view of small pores	35
Figure 4.12	Cross-sectional view of small pores	35
Figure 4.13	Thin-section of micrite	37
Figure 4.14	Thin-sections of sparite	38
Figure 4.15	Thin-sections of a polymictic conglomerate	39
Figure 5.1	Sequence of mound formation	49
Figure A.1	Microprobe photos of sample A1 and A4	53
Figure A.2	Microprobe photos of sample A5	54
Figure A.3	Microprobe photos of sample A6	55

Table of Tables

Table 2.1	Folk (1962) classification scheme	8
Table 2.2	Dunham (1962) classification scheme	8
Table 2.3	Types of porosity	9
Table 4.1	Percentage of carbonate	29
Table 4.2	Mole percentage of FeO, SrO, MgO and CaO	41
Table 5.1	Summation of mound features and interpretation	47

Acknowledgements

I wish to thank Peter Wallace for his excellent supervision, support of my ideas, and encouragement throughout the project. I wish to thank my family and friends for their support and understanding. I would like to give special thanks to the other three members of The Fabulous Four, Joe Kidston, Adam Layman, and Camilla Melrose, for their help during the late nights.

Chapter 1: Introduction

1.1 Introduction

Bay St. Lawrence fishermen have dredged up many fragments of odd shaped mounds along their fishing routes, structures that they believed to be a form of deep sea coral. In reality they are carbonate structures, most likely of non-biological origin, occurring in glaciomarine sediments and till 14.3Ka to 12.2Ka in age (Josenhans *et al.*, 1990). The carbonate structures show many dissimilar and similar characteristics to the well-studied carbonates in the rock record. One of the intriguing possibilities is that these mounds may be forming from localized geochemical processes, such as gas seepage. This project involves the characterization and interpretation of the previously unstudied deep sea carbonate structures, within the limits of hand sample observations, petrographic analyses, microprobe analysis and literature searches.

1.2 Purpose

The main objectives of this study are the following:

- 1) To characterize the carbonate structures.
- 2) To study and utilize previous works on related structures.
- 3) To perform an interpretation of the carbonate structures.
- 4) To provide a foundation that will encourage further studies on the carbonate structures.

1.3 Location and Distribution

The carbonate mounds occur offshore of the Bay St. Lawrence in Northern Cape Breton Island (Figure 1.1). The fishermen described the distribution to be localized on a small linear ridge covered by recent mud in a depth range of 160 – 210m. Fisherman have mapped out the extent of the mounds, occurring between UTM coordinates (5930-X-14578.5, 5930-Y-28810.0) and (5930-X-14581.5, 5930-Y-2811.0). This locality is about 5km NW of the Bay St. Lawrence and covers an area with a 2km radius.

1.4 Surficial Geology and Geomorphology

Figure 1.1 summarizes the glacial stratigraphy of the Gulf of St. Lawrence. Josenhans *et al.* (1990) identified that glacial retreat between 14.3Ka and 12.2Ka formed the late glacial stratigraphy of the Gulf of St. Lawrence. Most ground ice retreated rapidly north beyond Anticosti Island by 13.7Ka, however some residual piedmont lobes of ice remained until 12.2Ka. The Bay St. Lawrence to the Laurentian Channel was subject to a residual lobe, depositing glacial till overlain with glaciomarine sediments and reworked sands.

The till unit has a draped architecture ranging from 20 to 50m in thickness. The till unit is massive, dark grey, faintly laminated clayey mud with limestone and black slate clasts and igneous fragments. The glacial till overlies the underlying bedrock or older till units from the same glacial episode. Josenhan *et al.* (1990) interpreted the underlying bedrock to be Late Devonian to Early Carboniferous sedimentary rocks.

Glaciomarine sediments, as described by Josenhans and Lehman (1999), occur at the sea floor, ranging from 0 to 30m in total thickness in this region. The first sequence of

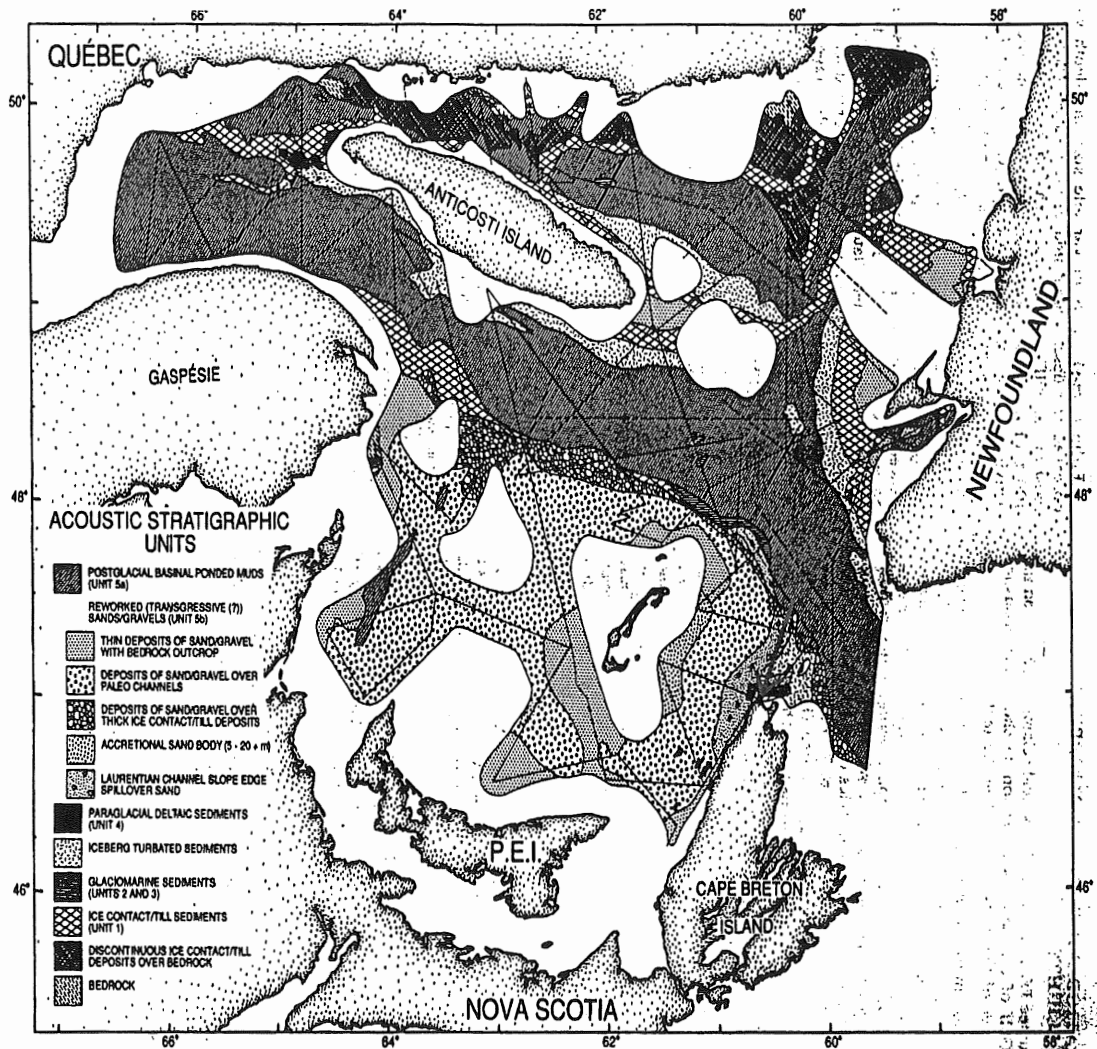


Figure 1.1: An overview of the glacial stratigraphy of the Gulf of St. Lawrence (Josenhans *et al.*, 1990). The red arrow indicates the location of the mounds.

glaciomarine sediment is laminated silty clay, with pebbly clasts. Interpreted to be deposited by bedloading and ice-rafting, this sequence drapes over the underling till. The next sequence of glaciomarine sediment is moderately stratified and interpreted to be ice distal sediment deposited by fresh water plumes emulating from the retreating ice margin. This unit is brown clayey mud with occasional pebbles. The final sequence of glaciomarine sediment is unstratified iceberg turbate. Compositionally, the iceberg turbate includes both underlying glaciomarine deposits and some glacial till in shallow areas. The iceberg turbate sediment does not occur deeper than 440m. Weakly stratified reworked sands from postglacial transgression occur at the seafloor surface where glaciomarine sediments were not deposited. This unit is grey clayey to sandy bioturbated mud with occasional shell fragments. This unit is often affected by gas venting pockmarks, forming up to 15m deep depressions on the seafloor surface (Fader 1991).

Quaternary sediments of the Bay St. Lawrence area experienced intense reworking in many localities in the past 100 years. Intensive fishing practices using dredging and trawling nets have scoured the seafloor surface. Many trawling scours incise the muddy seafloor to a depth of 1.5m. The trawl marks occur over hundreds of meters in length, oriented in both an east-west and north-south fashion, and at depths up to 200m.

1.5 Scope

The samples of carbonate mounds used for the characterization in this study were removed from the sea floor by dredging and trawling nets used by fishermen from Bay St. Lawrence. Samples characterized originate from the Bay St. Lawrence area, but have

actually no geographic referenced point. Characterization of the carbonate structures is limited to hand sample observations, petrographic analyses and microprobe data.

Petrographic studies consisted of studying 5 thin sections.

1.6 Organization

Chapter 2 is a background chapter for this study, including the relevant aspects of the literature search. A detailed literature search provides a basis on which to describe and interpret the previously unstudied carbonate mounds. Chapter 3 is the methodology. Chapter 4 is the characterization of the carbonate structures, providing hand sample observations and petrographic analysis results. Chapter 5 is an interpretation and discussion of the carbonate structures based on the results from Chapter 3 and Chapter 4. Chapter 5 focuses on classifying and identifying the carbonate structures. Chapter 6 presents the conclusions of this study and the recommendations to further this study.

Chapter 2: Background

2.1 Introduction

The carbonate mounds that are the focus of this study occur at 160-210m depths in marine water, 5km NW of Bay St. Lawrence, Cape Breton Island. The samples of these mounds can not be simply characterized as a carbonate rock, a carbonate mud mound, or carbonate concretion, due to a centimeter-scale diverse variability in morphology, texture and structure. A brief review of the relevant carbonate classifications is necessary, and will provide a basis for characterization of the carbonate mounds in this study.

2.2 Carbonate Classification

The Folk (1959) classification scheme characterizes carbonates according to the grain type and the matrix and cement. Folk (1959) separates limestones according to their allochemical components, carbonate grains that were transported and deposited as clasts, and their orthochemical components, carbonate grains that are deposited where they formed or that have been transported only a short distance. Four allochemical components were identified: (1) intraclasts, (2) ooids, (3) bioclasts and (4) peloids. Two primary orthochemical components were identified: (1) micrite, calcium carbonate mud, and (2) sparite, carbonate cement of interlocking clear crystals. Folk (1962) expanded his scheme to include crystalline carbonates where grains are unidentifiable. Table 2.1 classifies limestones according to textural maturity and proportion of allochems. Folk

(1962) further defined orthochemical components in carbonate rocks by paralleling micrite with mud matrixes in clastic rocks and sparite with cements in clastic rocks.

The Dunham (1962) classification scheme provides a framework for carbonate characterization based on depositional textures. Table 2.2 categorizes carbonate rocks into six categories based on the following textural features: abundance of carbonate mud, grain abundance, and occurrence of organic binding. Embry and Klovan (1971) provided a modified Dunham classification scheme that further categorizes coarse-grained carbonates and organically laminated boundstones. The Dunham (1962) and Embry and Klovan (1971) classification schemes ignore grain type, therefore greater specificity is achieved if grain type is also classified (i.e. a peloidal grainstone).

Schemes proposed by Folk (1959; 1962), Dunham (1962) and Embry and Klovan (1971) can not be fully applied to the characterization of the carbonate samples in this study for two reasons: (1) absence of a major allochemical component and (2) variability in calcium carbonate texture. However, orthochemical components outlined in the Folk (1962) scheme can be applied in the description of the calcium carbonate cement of the samples.

2.3 Porosity

Choquette and Pray (1970) define total porosity as the ratio of the total pore space to total volume of the rock, usually expressed as a percentage. Porosity is classified on four different elements: (1) basic porosity type, (2) origin of the porosity (3) the pore size and shape and (4) abundance. Table 2.3 lists the various porosity types outline by Choquette and Pray (1970). Two types prove relevant to this study: (1) channel porosity and (2) boring porosity. Channel pores are elongate with a length 10 times the width.

	OVER 2/3 LIME MUD MATRIX				SUBEQUAL SPAR & LIME MUD	OVER 2/3 SPAR CEMENT		
	0-1%	1-10%	10-50%	OVER 50%		SORTING POOR	SORTING GOOD	ROUNDED & ABRASED
Percent Allocations								
Representative Rock Terms	MICRITE & DISMICRITE	FOSSILIFEROUS MICRITE	SPARSE BIOMICRITE	PACKED BIOMICRITE	POORLY WASHED BIOSPARITE	UNSORTED BIOSPARITE	SORTED BIOSPARITE	ROUNDED BIOSPARITE
Terminology	Micrite & Dismicrite	Fossiliferous Micrite	Biomicrite		Biosparite			
Terrigenous Analogues	Claystone		Sandy Claystone	Clayey or Immature Sandstone	Submature Sandstone	Mature Sandstone	Supermature Sandstone	



 LIME MUD MATRIX
  SPARRY CALCITE CEMENT

Table 2.1: Limestone classification scheme based on textural maturity (Folk, 1962).

Depositional texture recognisable				Original components bound together	Not recognisable
Contains mud		Grain-supported	Lacks mud and is grain-supported		
Mud-supported					
less than 10% grains	more than 10% grains				
MUDSTONE	WACKSTONE	PACKSTONE	GRAINSTONE	BOUNDSTONE	

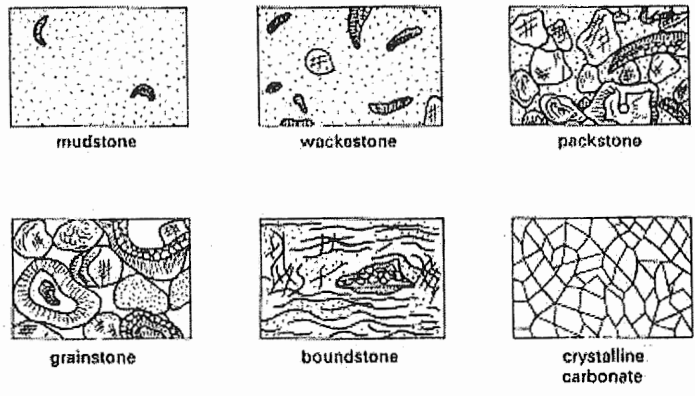


Table 2.2: Dunham's (1962) limestone classification scheme based depositional characteristics.

Boring pores are formed from boring and may present a large range of morphologies based on the boring organism.

Table 2.3: Porosity types defined by Choquette and Pray (1970)

Fabric selective	Not fabric selective	Fabric selective or not
Intergranular	Fracture	Breccia
Intragranular	Channel	Boring
Mouldic	Vuggy	Burrow
Fenestral	Cavern	Shrinkage
Shelter	Stylolitic	
Framework		

2.4 Carbonate Mud Mounds

The term carbonate mud mound can be defined as a carbonate buildup composed dominantly of carbonate mud, peloidal mud or micrite mud, and having some sort of depositional relief (James and Bourque, 1992). Carbonate mud mound relief is an arbitrary assessment. Relief can be low, less than 5 m of original topographic relief, or relief can be high, more than 5m of original topographic relief (Riding, 2002). Bosence and Bridges (1995) recognize 2 major varieties of carbonate mud mounds: (1) microbial mud-mounds, in which texture, composition and microfabric are thought to be *in situ* microbial in origin, and (2) biotrital mud-mounds, in which composition is a result of broken and transported skeletal debris. In Figure 2.1 Bosence and Bridges (1995)

categorize the variation and similarity between carbonate mud mounds and carbonate reefs through a triangular diagram, in which three end members are specified. This form of categorization only acknowledges carbonate buildups of biological origin (detrital or microbial). Numerous carbonate mud mounds have been characterized that lack a skeletal component. Wood (2001) defines these as complex autochthonous micrite-supported systems that are either organomineralic deposits (carbonate precipitation a result of abiotic organic substrates) or varieties of microbialite deposits (carbonate precipitation mediated from the activities or decay of biotic organisms). Riding (2002) adopts the definition of James and Bourque (1992) and argues that carbonate mud mounds form from a variety of processes, both organic and inorganic, which may be difficult to distinguish.

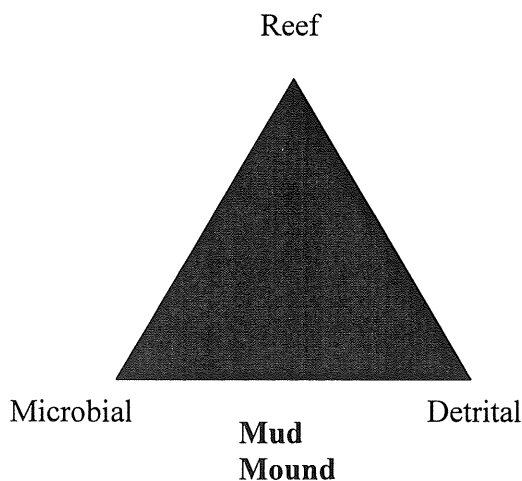
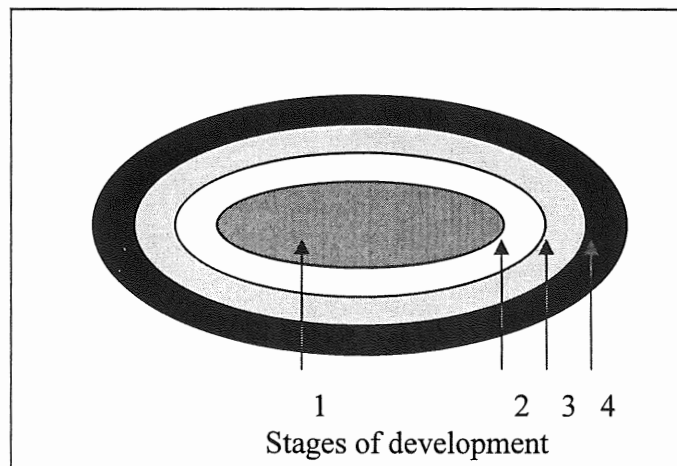


Figure 2.1: Bosence and Bridges (1995) use a triangular diagram to classify carbonate buildups according to three end members: reefs, microbial mud mounds and biodetrital mud mounds.

2.5 Concretions

Concretions are concentric mineralizations that occur in a sedimentary host rock (Mozley, 1996). Morphology is typically spherical or ellipsoidal, but can also be lobate or discoidal (Pratt, 2001). Numerous minerals can form as a concretion (e.g. siderite, iron oxides, manganese, apatite), but carbonate concretions will be primarily discussed in this section. Carbonate concretions usually form when carbonate material (fossils) in sediment layers act as a site of nucleation for calcite in the groundwater (Curtis and Coleman, 1986). The internal structure of a carbonate concretion is characterized by detrital carbonate material surrounded by concentric growths of authigenic microcrystalline and/or sparry carbonate (Gautier and Claypool, 1984). In Figure 2.2 Mozley (1996) outlines conventional concretion formation. Carbonate precipitates in a concentric manner by adding new carbonate to the outer edges of the concretion, resulting in older carbonate zones at the center of the concretion and younger carbonate zones at the outer edge. Macroscopic features of concretions are concentric internal layers, or systematic abrupt changes in the mineralogy, crystal size and/or crystal habit.

Figure 2.2: A hypothetical concretion outlined by Mozely (1996). Initial precipitation of the concretion began at the center (stage 1). The concretion grows when new material forms at the outer surface, resulting in concentric layers. The youngest zone of the concretion is stage 4.



Concretions often have chemical composition changes consistent with concentric growth patterns (Curtis and Coleman, 1986). Differences in concretion chemical composition are attributed to changes in pore-water chemistry during the period of concretion formation. Pratt (2001) associated concretions that formed from meteoric waters with a low Mg/Ca ratio and/or a high Sr/Ca ratio and concretions that formed from marine waters with a high Mg/Ca ratio.

Carbonate nodules are sedimentary structures similar to concretions. Carbonate nodules have a similar morphology with concretions, however internally nodules differ because they have no identifiable nucleus and internal structure.

2.6 Cold-Seeps and Carbonate Formation

Greinent et al. (2002) define cold-seeps as seafloor sites of fluid expulsion where authigenic minerals precipitate, most commonly carbonate, from a series of geochemical and biological processes. Carbonate precipitation is often associated with high methane concentrations, in which the carbonates are commonly Mg rich and have negative $\delta^{13}\text{C}$ values. Sulphate precipitates are also common in high methane areas. Chemoautotrophic fauna, such as chemoautotrophic worms and clams, contribute to carbonate precipitation at cold-seep sites. Bacterial or microbial mats also mediate large amounts of carbonate precipitation near cold-seeps. Fluid expulsion creates favourable chemical conditions for many organisms in localities that would normally prove unsuitable.

Carbonate formation is related to the rate and duration of the fluid expulsion (Roberts, 2001). Roberts (2001) associated rapid fluid expulsion with mud volcanoes and mud cones and slow fluid expulsion with seafloor lithification and mineral precipitates.

Carbonate precipitates at cold-seeps usually show a great variability and irregularity in morphology and structure due to the combination of both biological and geochemical processes (Greinent et al., 2002). Common authigenic carbonates include semicontinuous pavements of carbonate cemented sediments, circular carbonate chimneys, and carbonate slabs (Stakes et al., 1999).

2.7 Submarine Hardgrounds

Demmicco and Hardie (1994) define hardgrounds as a submarine sediment surface that was lithified by the ambient environment (depositional) before the next layer was deposited. Under this definition hardgrounds may have a wide variety of morphologies and structure, characteristic of the depositional environment and sediment layer. Demmicco and Hardie (1994) propose that early cementation of modern carbonate sediments can occur on shallow-water platforms to deep basinal environments.

2.8 Speleothems

Thraillkill (1976) termed speleothems to be termed chemically precipitated carbonates, characterized by their crystalline fabric. Thraillkill (1976) outlines several textures, including stalagmites, cave popcorn, moonmilk, and cave pearls. Cave popcorns are the structure most relevant to this study. They are defined to be knob-like structures with a gregarious nature. Their internal texture is defined by concentrically layered microcrystalline calcite. The concentric deposits are attributed to the depositional mechanism, which is a product of seepage and evenly distributed films by air.

Chapter 3: Methodology

3.1 Sample Collection

The six samples collected were received from fishermen of the Bay St. Lawrence area. The fishermen dredge up these fragments 5km NW off the Cape St. Lawrence. The fishermen state that the mounds occur on a ridge, within a 2km radius and at depths of 160-210m. The fishermen dredged up 21 fragments in the 2002 fishing season. Dates of when these structures were dredge and removed from the seafloor are undetermined.

3.2 Macroscopic Analysis

All 6 samples were macroscopically analyzed. An external analysis was performed to identify general morphologies and sedimentary features (both depositional and erosional). All 6 samples were sectioned for an internal analysis. Aims were to determine texture (grains, matrix and cement), composition (grains, matrix and cement) and sedimentary features (such as bedding or concentric layering). Attention was directed towards areas where textural or morphological changes occurred.

3.3 Petrographic Analysis

5 thin sections were used for the petrographic analysis: two from sample A1 and one each from A4, A5, and A6. The thin section areas measure about 20mm by 45mm. The focus of the petrographic analysis was calcite characterization in terms of crystal shape, habitat and episodes of precipitation.

3.4 Carbonate Percentage Determination

A dilute solution of HCL was placed in a beaker and both were weighed. A small weighed carbonate piece (< 0.1 g) from a sample was placed in the beaker. When the bubbling stopped, the beaker, residual liquid and residual sample were weighed. The mass of the carbonate in the sample is the difference in weight ((beaker + acid + sample) – (beaker + residual liquid + residual sample)) multiplied by the molar mass of the carbonate ion divided by the molar mass of CO_2 that was exsolved and dissipated in the air ($60.01/44.01$ g/mol). The percentage of carbonate was determined by dividing the mass of the carbonate by the mass of the sample and multiplying the result by 100.

3.5 Microprobe Analysis

The purpose of the microprobe analysis was to determine the chemical composition and chemical variability in the micrite and sparite. The microprobe used was model JEOL JXA – 8200 at Dalhousie University. The microprobe was prepared for carbonate analysis and related elements (i.e. Fe, Mg, Mn, Sr). Four samples were prepared for the microprobe analysis from four separate specimens: A1, A4, A5 and A6. Acceleration voltage of the microprobe was 15kV at a 10nA beam current. The counting interval was 20s. Selected areas of the samples were analyzed with a $10\ \mu\text{m}$ spot.

3.6 Hydrocarbon Detection

Samples were placed in a dark room and exposed to UV light. Organics (i.e. carbon) present reflect a deep-blue fluorescent light. Recorded were the colour, intensity and brightness reflected by the samples. This analysis is subjective and was used solely to detect if hydrocarbons were present.

Chapter 4: Results

4.1 Structures and Textures

4.1.1 Introduction

General morphology, size and colour of each sample are shown in Figure 4.1. In this section the surficial textures of each specimen is described. The subsequent descriptions can be used to categorize the samples into three textural types: (1) muddy, (2) popcorn and (3) erosional.

Muddy textures primarily occur massive and/or agglutinated. Agglutinated textures occur in specimens that have cemented silt to pebble sized siliciclasts and bioclasts. Some muddy units have a poorly defined layering, which do not have the agglutinated texture seen in the other specimens.

Samples categorized with popcorn texture have abundant clusters of popcorns on the surface. Popcorn is a textural term used to describe certain speleothem deposits (section 2.8), and is extensively used in this characterization. A popcorn can be identified as a bulbous or knobby extrusion from the body of the carbonate structure with a variable shape and size. The popcorn texture only occurs in samples A1 and A3. Surficial texture of popcorns is analogous with massive agglutinated mud. Samples with the popcorn texture also have polymictic conglomerate cemented in sparite at the surface.

Erosional texture is observed in all samples to some degree, however sample A4 and A5 are the only samples in which an erosional texture dominates. The erosional texture is divided into two types: (1) small tubular pores and (2) larger irregularly shaped pores. Pores are macroscopic features and are not fabric selective.

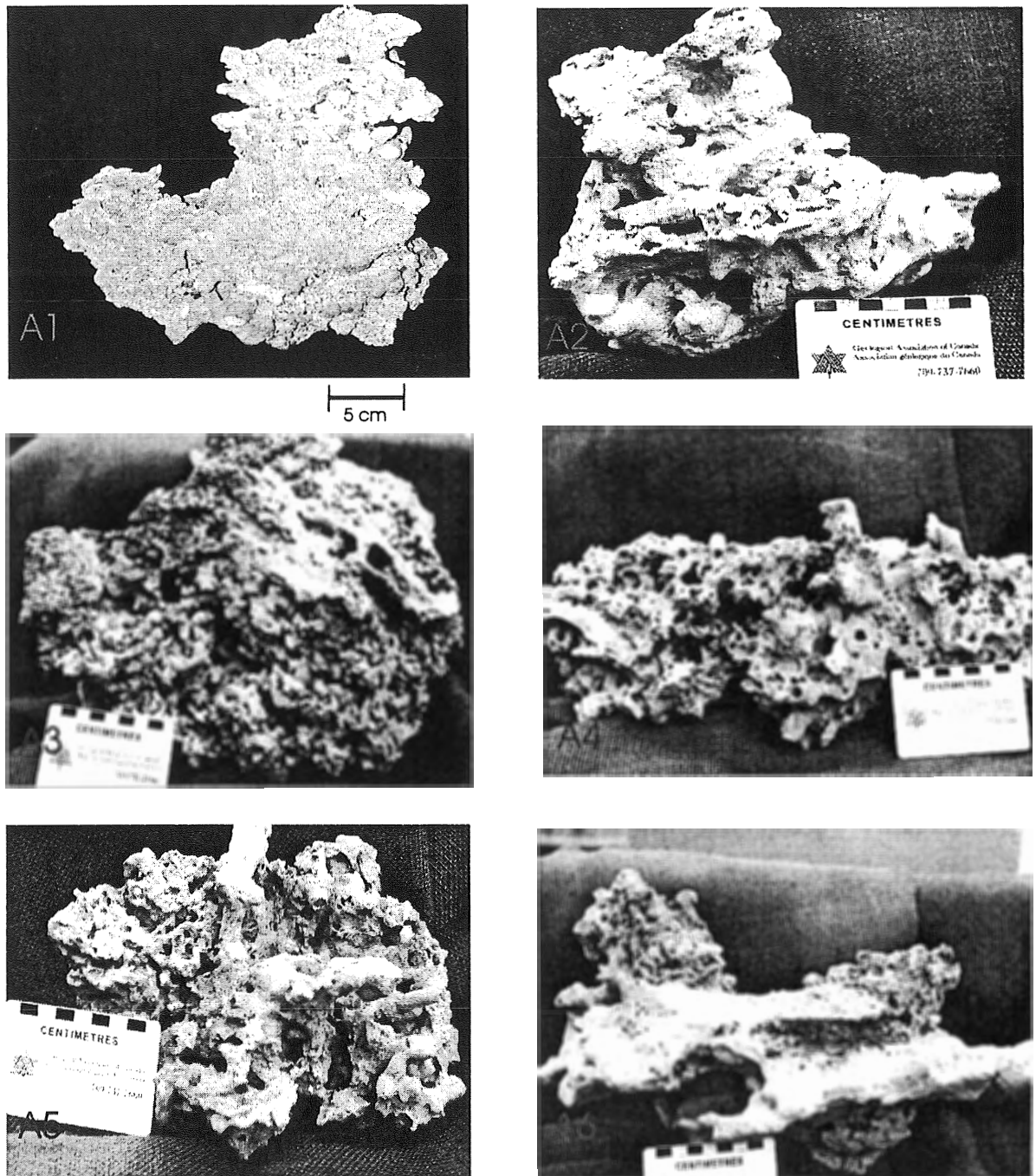


Figure 4.1: The six specimens characterized in this study. The carbonate structures are located between Loran-C coordinates (5930-X-14578.5, 5930-Y-28810.0) and (5930-X-14581.5, 5930-Y-2811.0), approximately 5km NW of Cape St. Lawrence and at 160 to 210m depth. Samples are labeled from A1 to A6. Each have been categorized according to their surficial texture. Sample A1 and sample A3 have been texturally defined according to their popcorn clusters. Sample A2 and A6 have a layered muddy texture. Sample A4 and sample A5 have many erosional features and have been defined accordingly.

4.1.2 Sample A1 - Popcorn

Four textures are identified on sample A1 in Figure 4.2a. The overall textural appearance can be categorized as popcorn, however there are components of massive agglutinated mud, polymictic conglomerate, and erosional pores. Popcorns have an ellipsoidal to spherical shape and occur elongated to knobby. Some popcorns branch apart or intertwine together, but the majority of popcorns occur as individual extremities. Popcorns can range in millimetres to centimetres in size. There is no apparent pattern in the distribution of the popcorn structures, however they cover about 60% of the mound. The popcorn structures occur with and are continuous with the muddy parts of the mound.

The popcorn structures and muddy parts in sample A1 have a massive and agglutinated texture. Siliciclastic grains, silt to pebble size, are cemented on the surface. Bioclasts are also cemented on surface, such as echinoid spines, bivalves and gastropods. No pattern in the distribution of bioclasts is identifiable. The abundance of pebble sized grains and bioclasts cemented in mud dominated textures is estimated at 10% (surface cover). The massive and agglutinated muddy texture covers about 50% of the surface, partially due to the large number of popcorn structures. Figure 4.2b shows some of the popcorn structures and muddy parts covered by a lens of sparry calcite. The lens of sparry calcite is estimated to cover 20% of the surface.

Figure 4.2c shows a polymictic conglomerate cemented in sparite, which is estimated to cover about 30% of the mound surface. Clasts range from various siliciclasts to bioclasts in composition and silt to pebble in size. Clast abundance is estimated at 30%. The conglomerate clasts are not sorted and no clast orientation can be inferred.

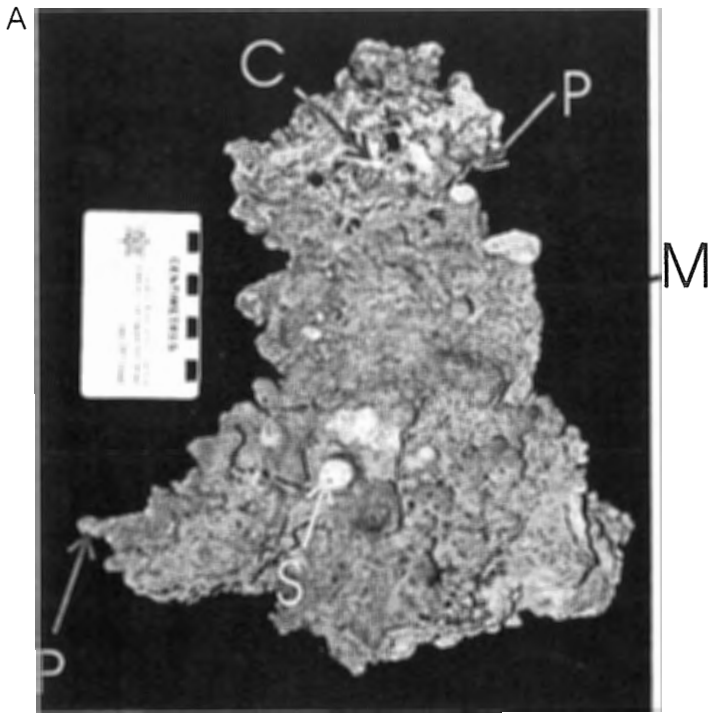
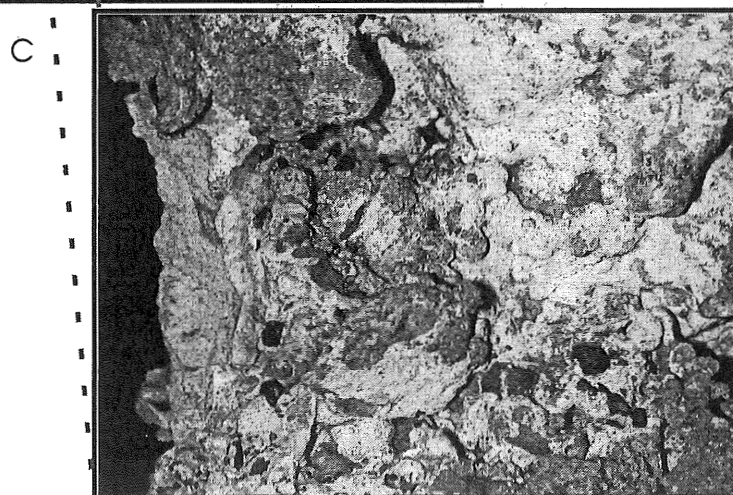
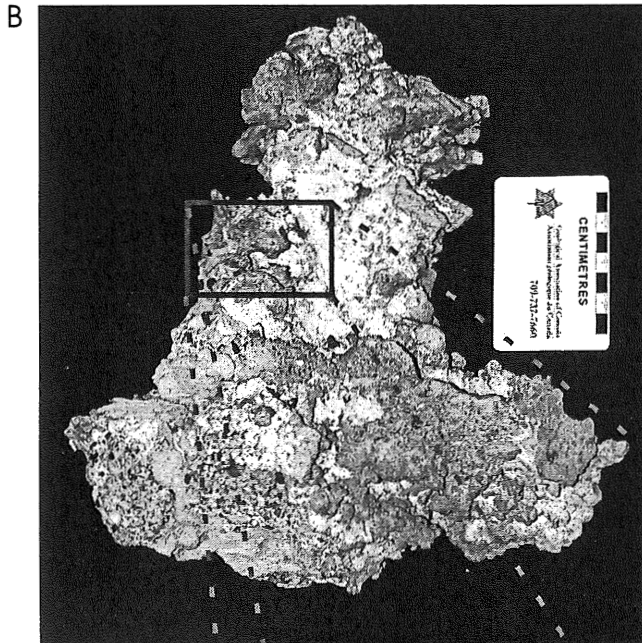


Figure 4.2: (A) Four surficial textures can be recognized on sample A1: (1) popcorn (P), (2) massive agglutinated mud (M), (3) polymictic conglomerate cemented in sparite (C), and small pores (S). (B) Part of the surface of sample A1 is covered by a layer of sparite (C) A macroscopic view of the polymictic conglomerate shows a sparry calcite cement and a few cemented shell fragments.



Small pores are found throughout the surface of the specimen (Figure 4.2a). The pores are very well-rounded and cylindrical to tubular shaped. Pore diameter on average is about 1mm in size, however there is a large variability in pore size. The apparent length to width ratio of the pores is about 5:1 to 15:1. An estimated percentage of porosity exposed on the surface is 30%. The small tubular pores occur on the agglutinated mud textures.

4.1.3 Sample A2 - Muddy

Sample A2 can be texturally classified as muddy with poorly defined layering. In Figure 4.3a the massive and homogenous nature of the muddy texture is shown. Cemented in the mud are various bioclasts, such as bivalves and gastropods. Bioclast abundance is estimated at about 5 to 10%.

Figure 4.3b outlines parallel layering in the sample. Layers have been identified as sections of carbonate mound that have been partitioned by a groove in the mound above and below the section. Layer thickness ranges from 1cm to 2cm, however no distribution or grading in layer thickness occurs. Large irregular shaped pores occur on the upper and lower margins of the layers (Figure 4.3a, Figure 4.3b). These pores are present within the body of the specimen, but are largely concentrated around layer margins. Pore openings have a deformed spherical to lobate shape ranging from 0.5cm to 2cm in diameter. Pores have a variable length to width ratio, ranging from 2:1 to 20:1. Some pores completely penetrate through the sample creating channel like holes. Small well-rounded tubular pores, averaging 1mm in diameter, are also found on this sample.

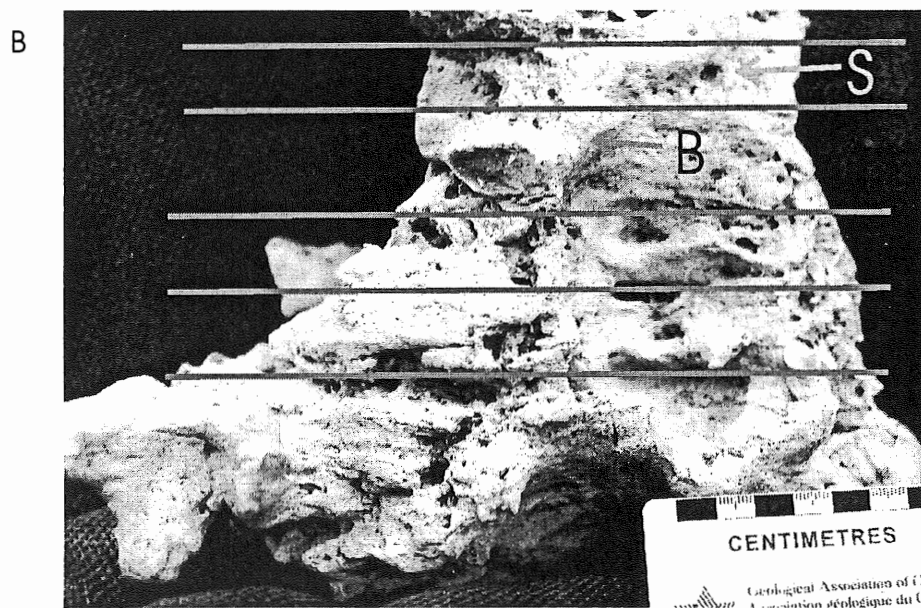
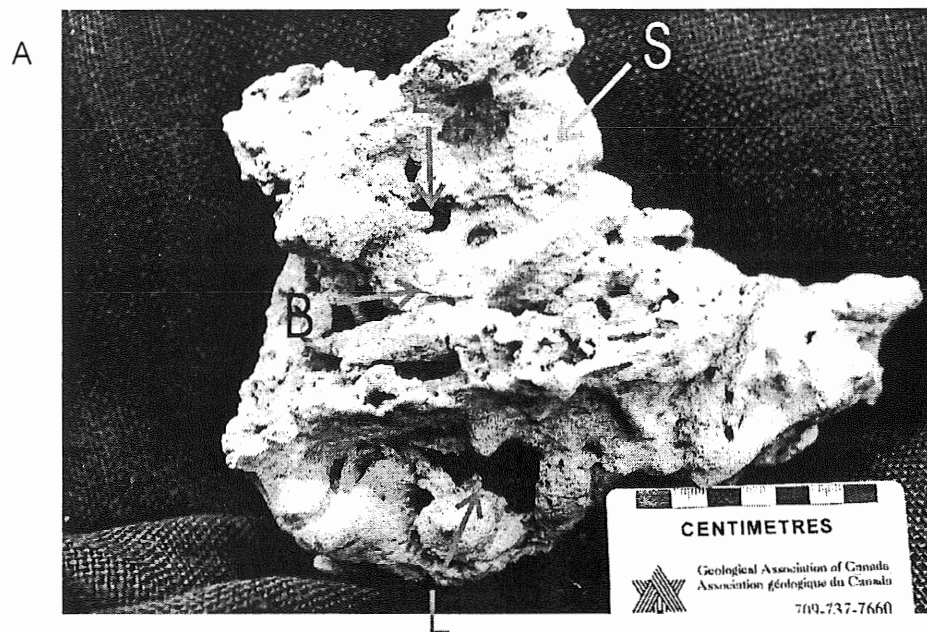


Figure 4.3: (A) Sample A2 has a layered muddied texture. Large pores (L) are mainly concentrated around layer margins. Small pores (S) are found throughout the mound. (B) Layering, outlined with red lines, is parallel. Several bioclasts are cemented to the surface (B).

These pores have a 5:1 to 15:1 length width ratio. Total porosity on this sample is estimated at 45%

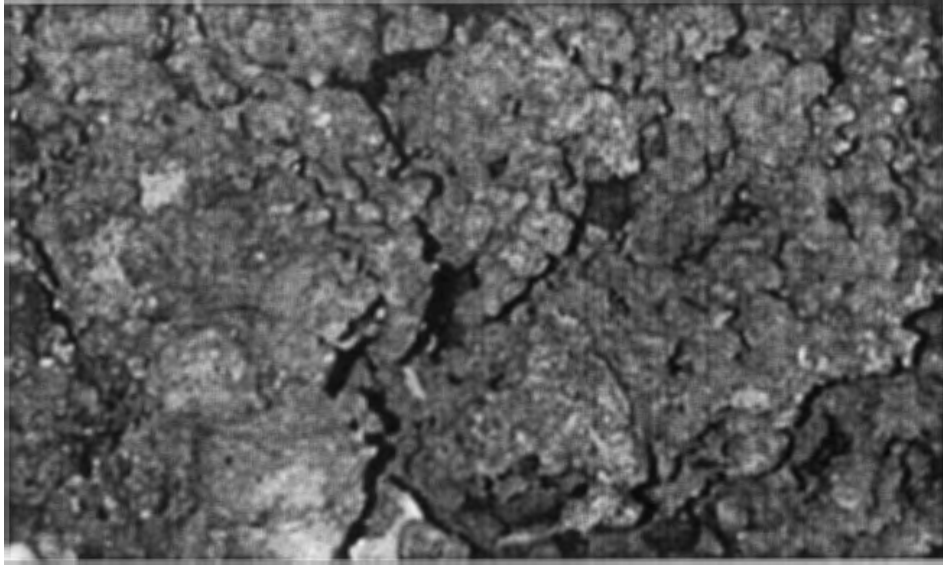
4.1.4 Sample A3 - Popcorn

Figure 4.4a illustrates the texture of sample A3. Popcorns cover about 70% of the sample surface. Popcorns are ellipsoidal and spherical in shape and range in size from millimetres to centimetres. Popcorns in sample A3 appear more 'developed' than the popcorns observed in sample A1. Popcorns in sample A3 are more elongated and form an extensive branching and intertwining framework. The surficial texture of the popcorns can be described as massive agglutinated mud. Siliciclastic sediment, silt to pebble size, and bioclasts are cemented on the surface of mud dominated textures. Abundance of pebble sized clasts and bioclasts is estimated at 10% (surface cover). No systematic distribution of clasts or bioclasts can be identified.

Figure 4.4b shows a polymictic conglomerate cemented in sparite. Conglomerate covers about 30% of the surface. The conglomerate is composed of various siliciclastic grains, silt to pebble size, and bioclasts. No preferred orientation or sorting can be inferred from the grains. Bioclasts are echinoids, bivalves and gastropods. No systematic distribution of bioclasts can be inferred. Abundance of clasts in the conglomerate is about 30 to 40%. Estimated abundance of bioclasts is 10%.

Total porosity of the sample is estimated between 5% and 10%. Small tubular pores occur on the surface of the sample, but are not abundant. Pores have an average diameter of 1mm and have a length to width ratio of 5:1 to 15:1.

A



B



1cm

Figure 4.4: (A) The surface of A3 is dominated by a popcorn texture, covering about 70% of the surface. (B) Polymictic conglomerate cemented by sparry calcite covers about 30% of the surface. Clasts are angular to subangular and poorly sorted. Several shell fragments (B) are cemented in the conglomerate.

4.1.5 Sample A4 - Erosional

This mound fragment is classified as having an erosional texture, based on the extensive network of large and small pores that makes the original texture difficult to define (Figure 4.5a). Figure 4.5a outlines coarse layering defined by differential erosion. The larger pores are identified in Figure 4.5b. The pore openings have a deformed spherical to lobate shape. Pore size ranges from millimetres to several centimetres. The length to width ratio of the pores is 1:1 to 10:1. Most large pores penetrate through the sample. Smaller pores are outlined in Figure 4.5b. These pores are well-rounded and tubular in shape. Pore diameter averages about 1mm, however pore size is largely variable. Many of the small pores penetrate through the samples. Total surface porosity is estimated at 70 to 80%. The uneroded part of the sample has a massive muddy texture. Very few cemented siliciclasts or bioclasts are present.

4.1.6 Sample 5 - Erosional

Similar to sample A4, this sample is categorized on the basis of erosional features. The actual sample body has a massive muddy texture. Analogous with sample A4, very few cemented bioclasts and siliciclasts are present.

Total porosity of the sample is estimated to be 50 to 60%. Large pores have deformed lobate to spherical openings and range from millimetres to several centimetres in size. Length to width ratio of the large pores is 1:1 to 20:1. The large pores often penetrate through the sample. The small pores have a tubular and cylindrical shape and are very well rounded. The small pores have an average diameter of 1mm, but pore size

A



B

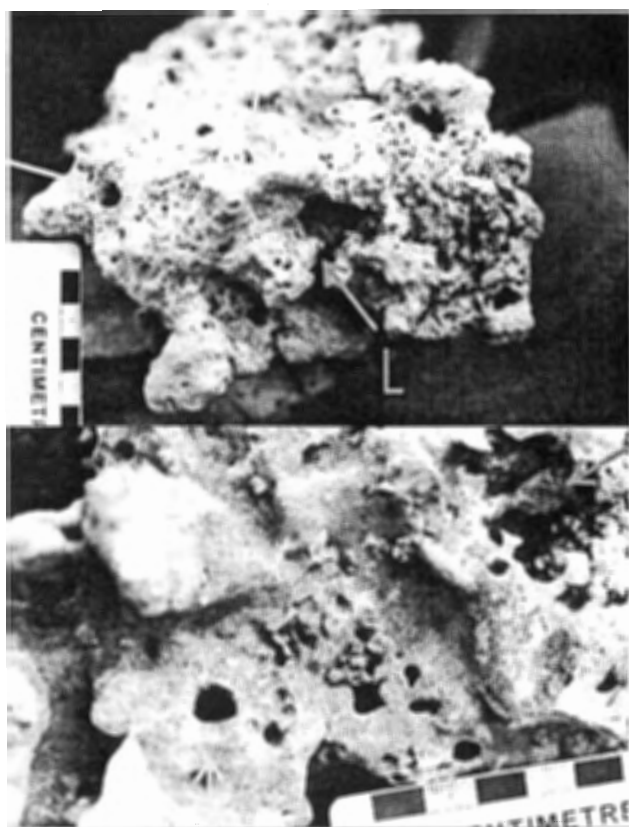


Figure 4.5: (A) Red lines outline the poorly defined layering in sample A4. Large (L) and small (S) pores are the primary textural feature of this specimen. (B) Large pores have lobate to ellipsoidal pore openings. Small pores have well-rounded tubular openings.

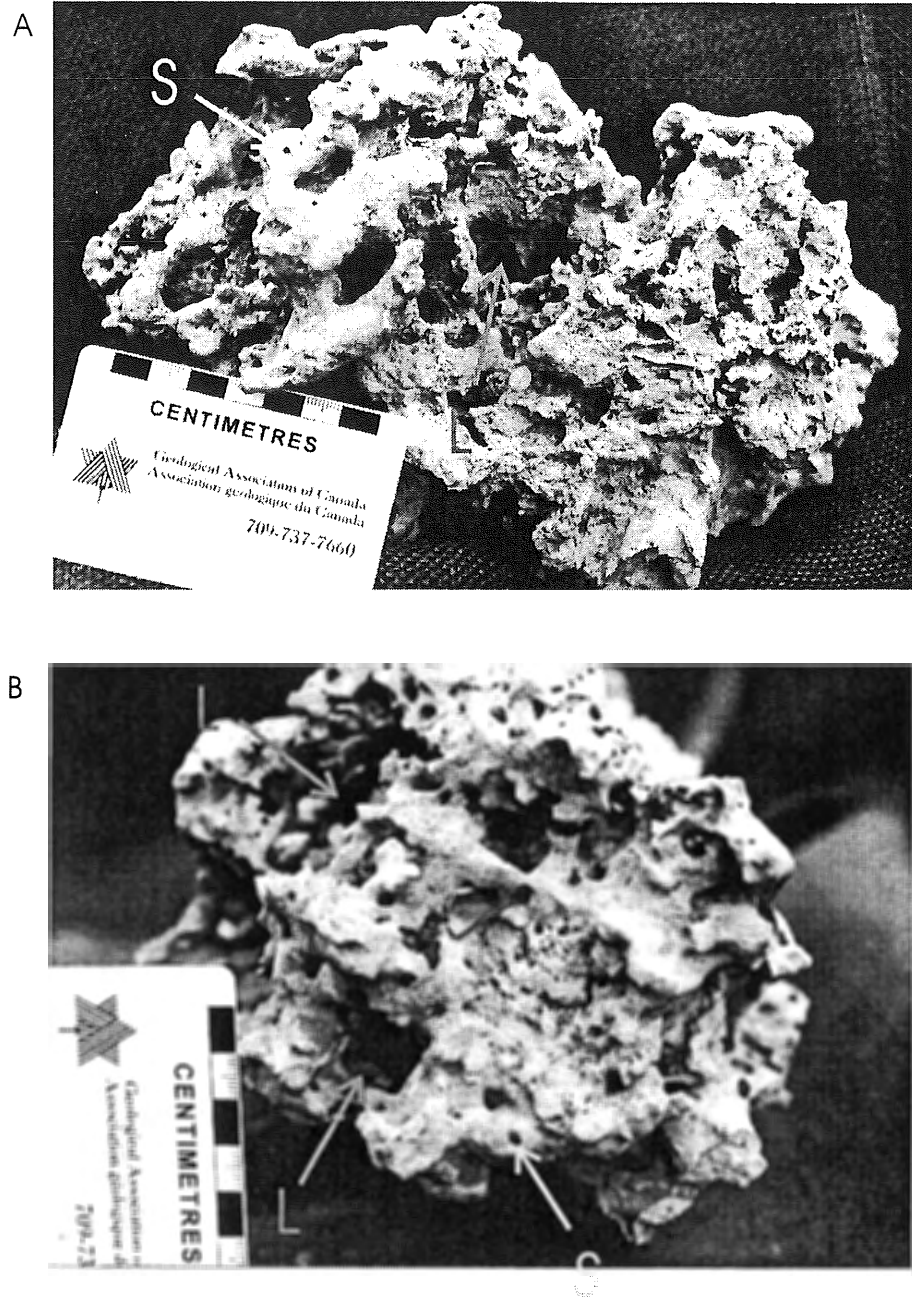


Figure 4.6: (A,B) Sample A5 is categorized according to its erosional features. Large pores (L) have deformed lobated to ellipsoidal pore openings. Small pores (S) are well-round and tubular. The actual mound body has a muddy texture.

can be up to 5mm. Length to width ratio of the small pores ranges from 5:1 to 15:1. Some pores completely penetrate through the sample.

4.1.7 Sample 6 - Muddy

Sample A6 is texturally classified as muddy. In Figure 4.7a parallel layering is identified. The platform type layers are parallel, which gives the sample a sheet-like morphology. The mud is massive and has very few clasts cemented to the surface. Clast abundance is estimated at less than 10%. Figure 4.7b shows gastropods cemented to the surface, representative of the bioclastic component (gastropods and bivalves). This sample has relatively large amount of bioclast material cemented to the surface, estimated at about 5 to 10%.

Large clumps of a muddy texture occur on one side of the specimen. These clumps are heavily eroded by large pores, shown in Figure 4.7a and Figure 4.7b. The large pores have deformed lobate to spherical pore openings and range in size from millimetres to centimetres. Their length to width ratio is 1:1 to 20:1 and the pores often completely penetrate through the specimen.

The massive mud sheets have numerous small pores, tubular and cylindrical in shape. The pores are well rounded and have an average diameter of 1mm. Length to width ratio of the small pores is 5:1 to 15:1. Total porosity is estimated at 50%

4.2 Carbonate Percentage

Each sample, except for sample A1, was tested for the percentage of carbonate. Samples A2, A3, and A4 were tested several times to determine if any variation in

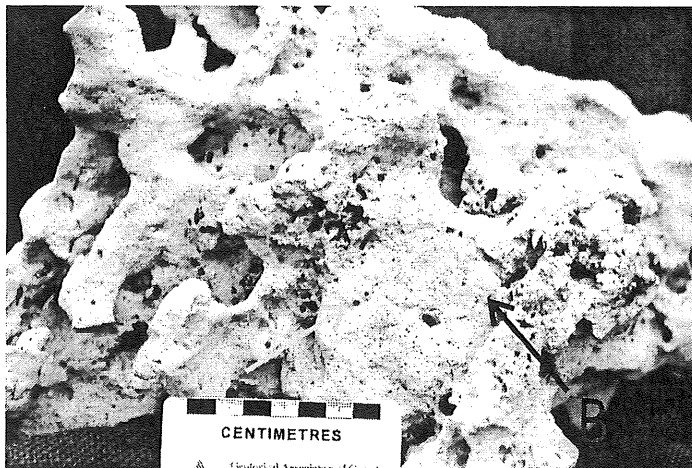
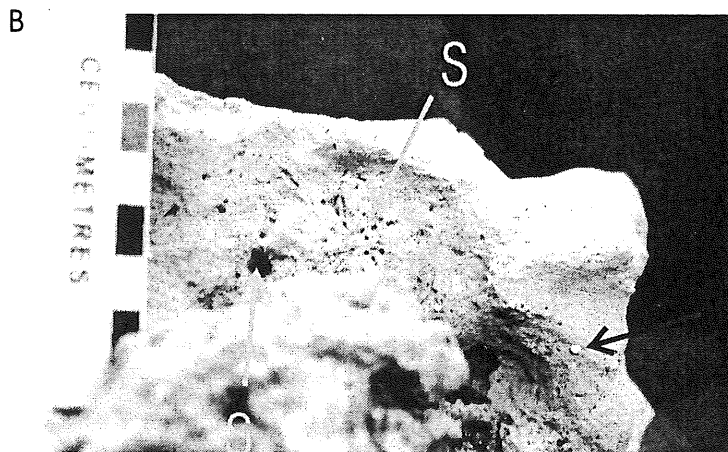
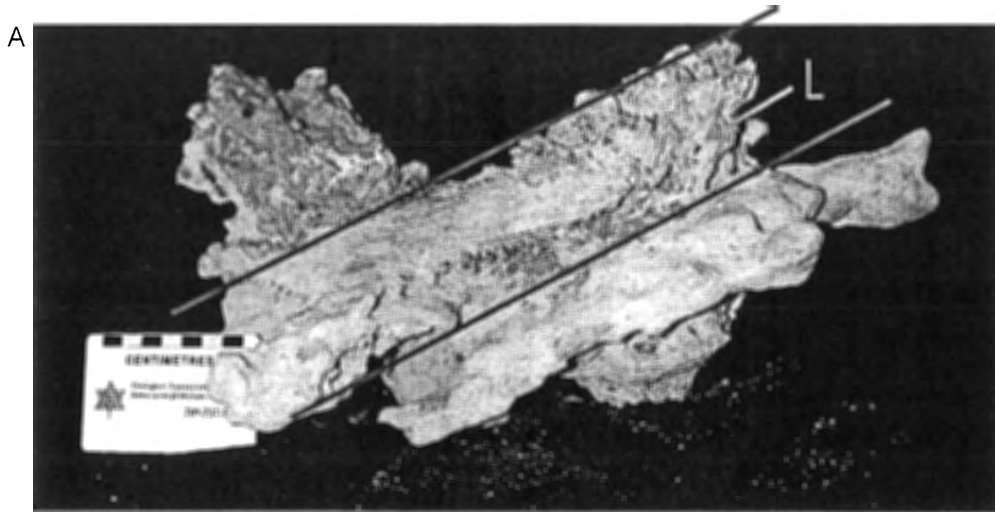


Figure 4.7: (A) Layering in sample A6 gives it a sheet like appearance (red lines). Clumps of porous mud occur on one side of the specimen. (A,B) Large pores (L) mainly occur on the large clumps of mud. Small pores (S) mainly occur on the sheets of mud. This specimen has a relatively large amount of cemented bioclasts (B).

carbonate percentage occurs within the samples. Carbonate percentages are presented in Table 4.1. The largest percentage of carbonate is associated with specimen A2, classified with a muddy layered texture. Samples with a popcorn texture and agglutinated muddy texture have a relatively low percentage of carbonate (Sample A3). Specimens defined with an erosional texture typically show a low percentage of carbonate (sample A4 and sample A5).

Two tests of sample A2 shows that variations in carbonate percentage can occur within one sample. Multiple testing of samples A3 and A6 show a relatively consistent percentage of carbonate.

Table 4.1: Determined carbonate percentage for each sample. Methodology used to determine carbonate percentage is outlined in section 3.4.

Sample	Carbonate Percentage (%)		
	Test 1	Test 2	Test 3
A2	95	62	N/A
A3	31	30	N/A
A4	46	N/A	N/A
A5	39	N/A	N/A
A6	34	33	42

4.3 Internal Textures and Structures

This section describes the textures, structures and their relationships of the carbonate specimens observed in cross-sectional views. In this section samples are not

A

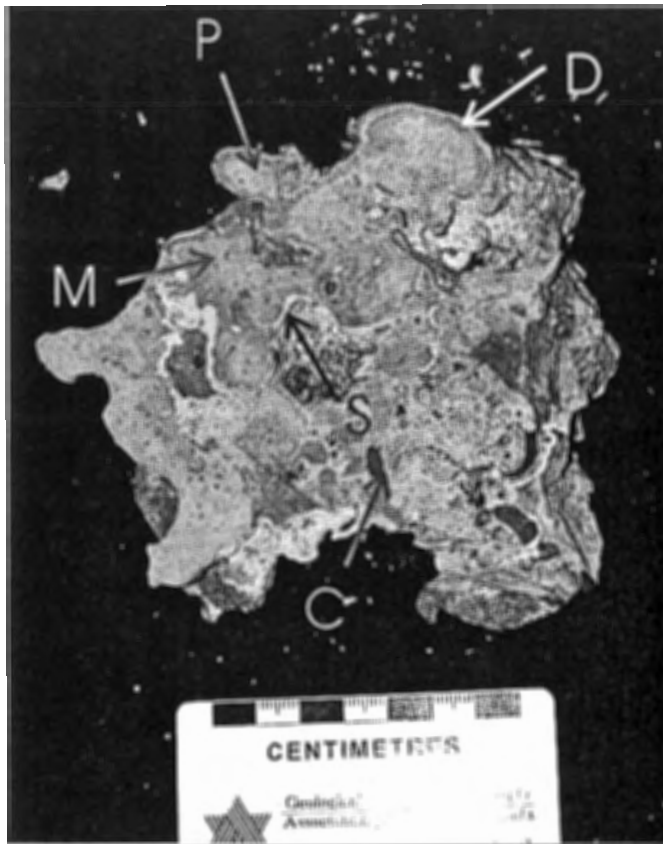
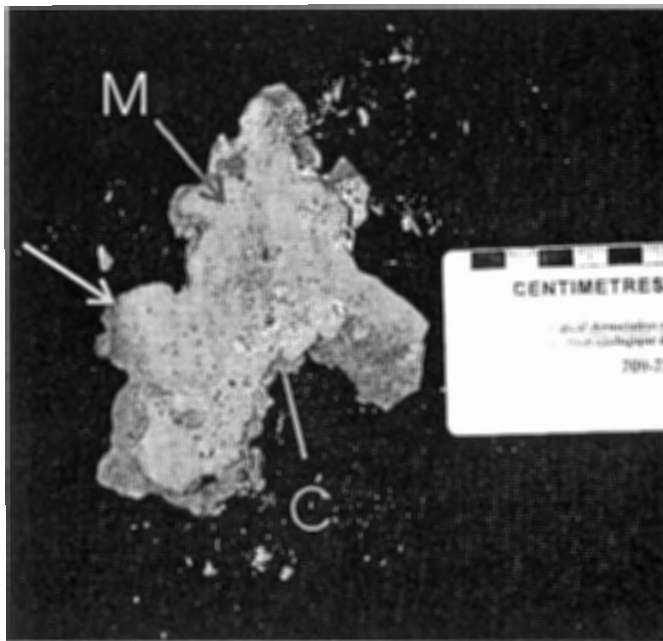


Figure 4.8: (A) A cross-sectional view of the carbonate specimens. Indicated is the distribution of the following features: lime mud (M), dark bands (D), polymictic conglomerate (C), sparite (S), and popcorn structures (P). (B) A cross-sectional view of the carbonate specimens. The conglomerate in the lower right part of the section has lime mud clasts.

B



described individually, but rather textures, structures and their relationships are described on a whole.

4.3.1 Distribution

Figure 4.8 is a typical cross-sectional view of a specimen. The core or body of the specimen is primarily lime mud. Popcorns and polymictic conglomerates are textures that solely appear on the surface. Sparite calcite is restricted to pore holes, polymictic conglomerates (sparite as the cement) and the surface of the specimens.

4.3.2 Lime Mud

Lime mud, grey in colour, is the primary internal component of the samples (Figure 4.8). The lime mud is fine grained to finely crystalline. The lime mud is rich with quartz. Quartz grains have an average grain size 0.1mm. The internal texture of the lime mud is finer grained than agglutinated mud characteristic of the surface of some samples. The internal texture is very homogenous throughout all the samples.

No internal lamination, allochemical component, or biological framework can be identified at this level of detail. Cemented shell fragments that occur within the body of the specimen have only been observed in sample A3. It is suspected that most bioclasts (bivalves, gastropods and echinoids) are limited to the surface of the mounds and are therefore a more recent feature.

In every mound a dark grey to black band of lime mud occurs at the perimeter of the structures (Figure 4.8a, Figure 4.8b). A dark band also occurs around pore holes and around the perimeter of the popcorns in sample A1. The dark bands have the same quartz-rich fine grained texture as other lime mud components. The bands measure about

0.5mm to 1mm in width. When placed under UV light the bands emitted a florescent purple light, suggesting the presence of organics.

4.3.3 Popcorns

In sample A1 the popcorns appear to be extrusions or extension of the lime mud because the internal texture is analogous with that of the lime mud (Figure 4.8). The popcorns in sample A2 do not have dark bands around the perimeter, but rather the entire internal colour is dark grey to black. The texture is analogous with the lime mud previously described. When tested with UV light the popcorn structures emitted a florescent purple light, suggesting the presence of organics.

4.3.4 Sparite and Polymictic Conglomerate

Figure 4.9 shows sparite occurring in pore spaces to have a radial to acicular form and to be concentrically banded. Some sparite that occurs in pore spaces or as cement in the polymictic conglomerate has a bladed form with no apparent banding (Figure 4.10). Sparite that occurs as the cement in the polymictic conglomerate has a drusy texture (Figure 4.10).

The polymictic conglomerate shows no preferred orientation or sorting of clasts in a cross-sectional view. The conglomerate is composed of various siliciclastic grains and intraclasts. Included are grains of lime mud composition (Figure 4.10), which have the same textural properties as the adjacent lime mud (Figure 4.8b). Lime mud clasts are angular to subangular and range 0.5mm to 2mm in size. The presence of lime mud clasts

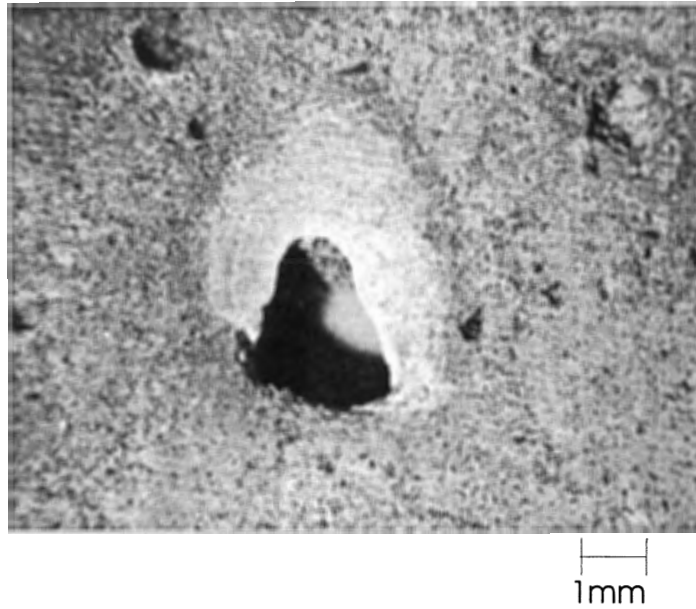


Figure 4.9: Concentrically banded sparite in a pore hole. Sparite has an acicular to radial form.

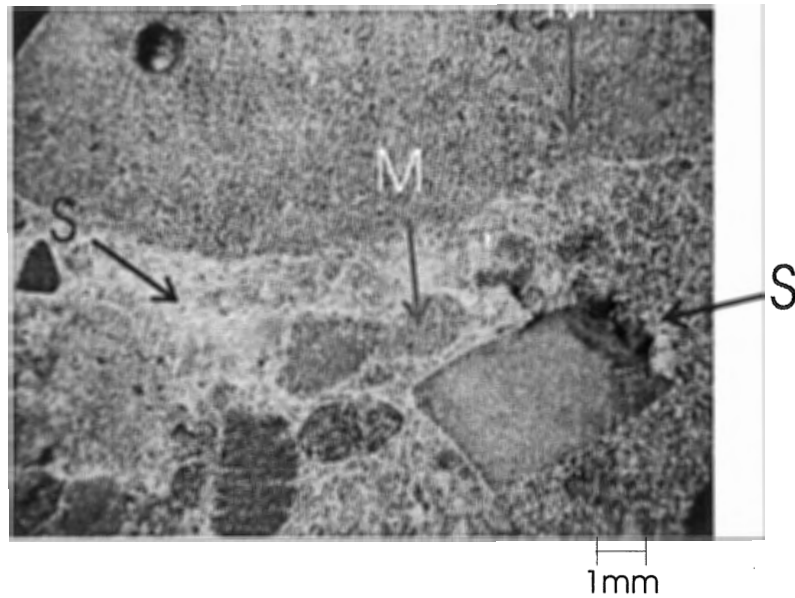


Figure 4.10: Sparite has both a blocky and a bladed crystal form in the polymictic conglomerate. Lime mud clasts occur in the polymictic conglomerate.

suggests that some brecciation accompanied with sparite precipitation may have occurred.

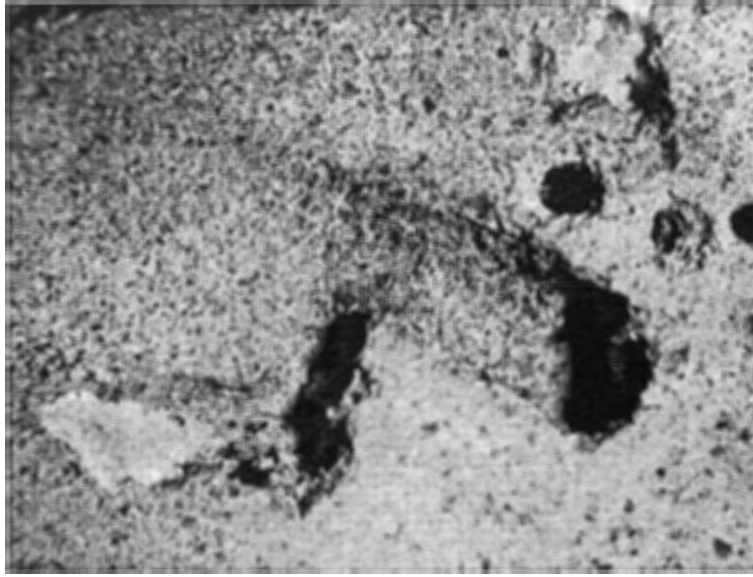
4.3.5 Small Pores

The small pores are an erosional feature that is extensively found on all samples. The average pore size is about 1mm in diameter. The pores have a tubular or cylindrical shape. The pores have been described as very well-rounded, which means that the interior pore walls are very smooth and consistent. Figure 4.11 is a cross-sectional view of a pore, indicating that not all pores have a completely straight morphology. Some pores take directional changes of about 90°. These directional changes do not affect the integrity of the pore walls, which maintain very well-rounded. In figure 4.12 various pores have been filled in with lime mud.

4.4 Petrography

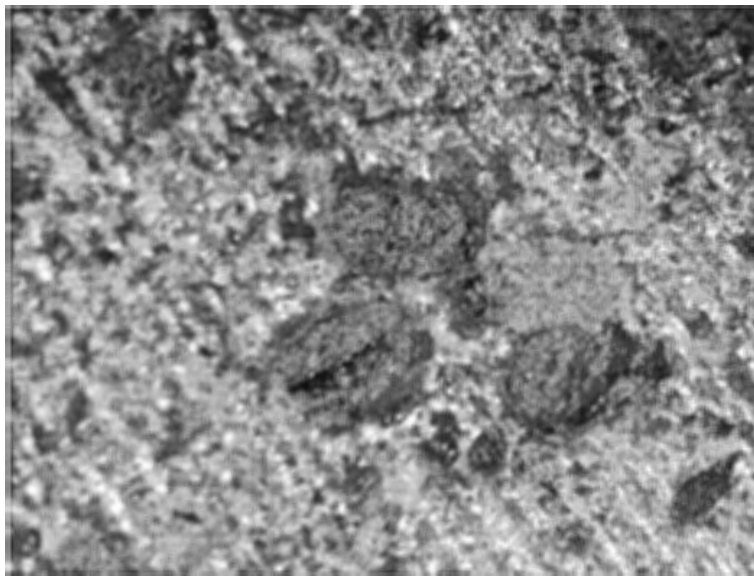
4.4.1 Micrite

Micrite occurs in two localities: (1) in the lime mud areas of the samples (the body or core) and (2) in the lime mud clasts in the conglomerate. In Figure 4.13 a dark and a light brown micrite material is identified. The dark brown micrite is cryptocrystalline, although the actual fabric is difficult to distinguish. The term micrite-grade material has been used by Chafetez and Folk (1984) to describe mud-rich and texturally undefined micrite, and may prove to be the most appropriate term here. The micrite-grade material is quartz rich, supporting numerous of quartz grains 0.1mm – 1mm in size.



1mm

Figure 4.11: A cross-sectional view of a small pore hole. The pore changes direction several times, but the interior integrity of the pore is maintained. Sparite has precipitated at the end of the pore.



1mm

Figure 4.12: Several pores are filled in with lime mud.

Light brown micrite is finely crystalline with a radial to fibrous fabric. The light brown micrite does not support quartz or any other grain types. The light brown micrite occurs at the contacts of the dark micrite-grade material and sparite and has a drusy texture. These localities are at the perimeters of the samples, on surface of pore holes and in the lime mud clasts. It should be noted that there are contacts between dark micrite-grade material and sparite where the light brown micrite is not present.

Lime mud clasts have both light brown micrite and dark brown micrite-grade material. The segregated clasts have a peloidal-like texture if there is large abundance of the fibrous to radial light brown micrite (Figure 4.13).

4.1.2 Sparite (and polymictic conglomerate)

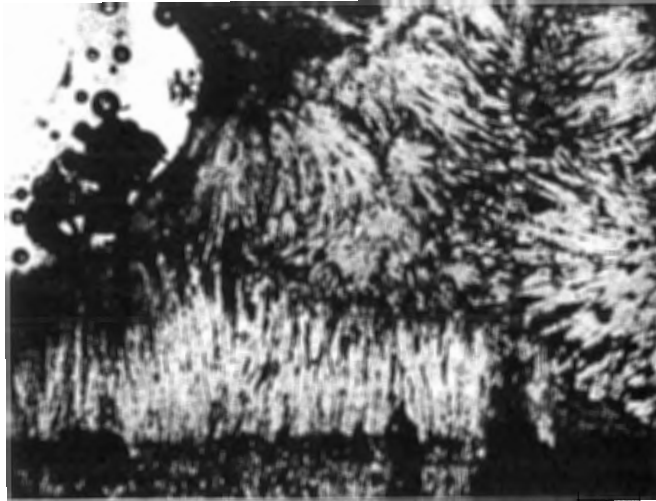
As previously mentioned, sparite occurs in a variety of crystal forms. Figure 4.14a shows sparite in a pore space. Sparite crystals are elongate with a 10:1 to 15:1 length to width ratio. The crystal form can be characterized as radial to bladed. Figure 4.14b shows sparite from a pore space. This sparite has a length to width ratio of 8:1 to 10:1. Crystal form can be characterized as radial. In Figure 4.14c, a concentrically banded acicular sparite is shown. This sparite occurs on the surface of mound. Crystal length to width ratio is 3:1 to 8:1.

No relationship between sparite crystal form and locality could be inferred. Sparite occurs acicular, radial, and bladed in both pore spaces and on the surface. Concentrically banded sparite occurs both on the surface and in pore spaces.

Figure 4.15 shows a polymictic conglomerate in cross-sections, which truly emphasizes the variability in clast composition. The sparite cement has a bladed crystal



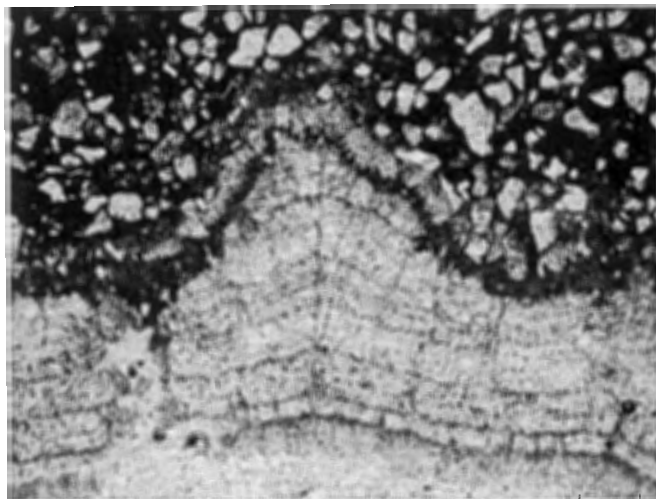
Figure 4.13: Two types of micrite are identified: (1) dark brown micrite-grade material (DM) and (2) light brown micrite (LM). The dark brown micrite-grade material is quartz rich (Qtz). Lime mud clasts have both types of micrite. Clasts with a large component of light brown micrite have a peloidal-like texture (P).



1mm



1mm



1mm

Figure 4.14: Three thin-sections of sparite. (A) Sparite occurring in a pore space. The sparite has a radial to bladed crystal form. (B) Sparite occurring in a pore space. The sparite has a radial crystal form. (C) Sparite occurring on the surface. The sparite has an acicular crystal form. The sparite is concentrically banded.

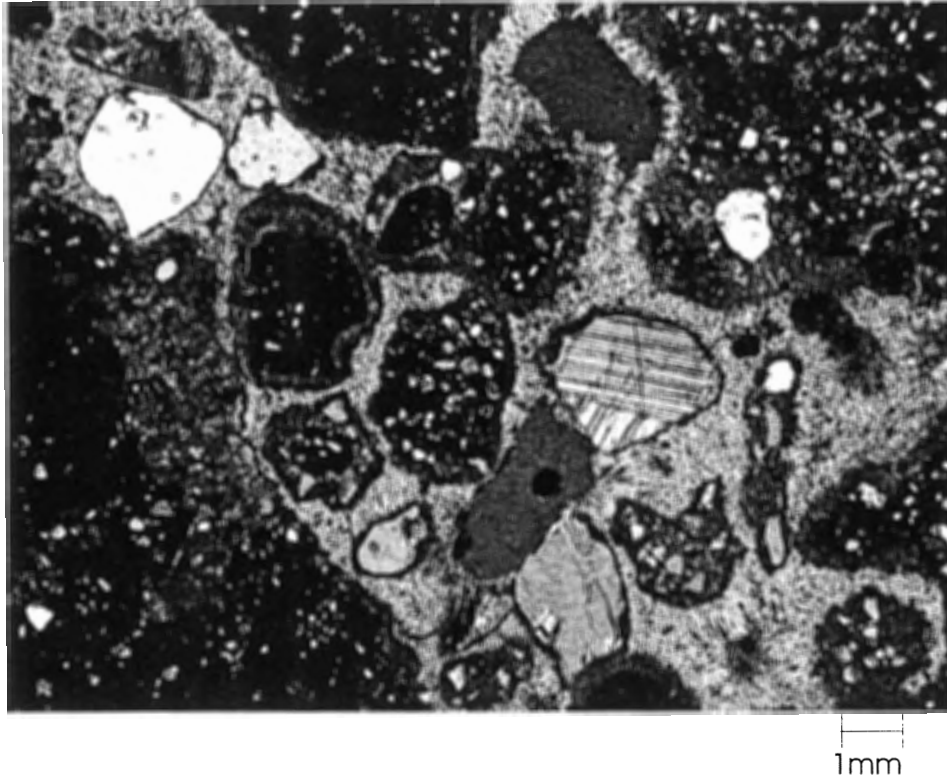


Figure 4.15: A thin-section of polymictic conglomerate. The variability of clast composition is truly emphasized in XN. The sparite cement has a bladed crystal form. The overall cement texture can be described as drusy.

form. The length to width ratio of sparite crystals is 5:1 to 10:1. The overall cement texture can be termed drusy.

4.5 Microprobe analysis

Microprobe results are not accurate because a 10 μ m spot was too large for the analysis. The muddy and clastic nature of the carbonate specimen resulted in many background materials being included in the analysis that can not be calculated out. When testing micrite-grade material, substantial amount of aluminium oxide and silica oxide were counted. Because other minerals associated with aluminium (i.e. K) were not tested, aluminium and silica can not be calculated to achieve precise carbonate chemistries. This also means that the levels of Mg, Fe and Sr, elements commonly associated with carbonate, may partially be associated with background material. Regardless of the restrictions on the data, relative amounts of Mg, Sr, and Fe can be discussed. Table 4.2 presents percentages of FeO, MgO and SrO relative to CaO of all the carbonate spots tested. Appendix A is the maps of sample spots. Appendix B is the complete data set of the microprobe analysis.

Spots A1-1 to A5-5 analyzed clast composition. The majority of large clasts in the micrite-grade material are quartz (Appendix A1). All other spots were focused on carbonate compositions, except spots A5-7 to A-12 which tested a shell. Both sparite and micrite-grade carbonates have relatively low levels of Fe. The micrite-graded material has relatively low levels of SrO. The ratio of Mg/Ca in micrite-grade material can be interpreted to be less than 5%, which means the micrite has low level of Mg. Sparite has relatively high Sr levels, with ratio of Sr/Ca between 0.4 and 1%.

Table 4.2: Mole percentage (of mass) of FeO, MgO, SrO and CaO in the carbonate samples. Sample spots can be referred with Figure A.1, A.2, and A.3 in Appendix A.

<u>Sample</u>	<u>Mole Percent FeO</u>	<u>Mole Percent MgO</u>	<u>Mole Percent of SrO</u>	<u>Mole Percent of CaO</u>	<u>Carbonate Type</u>
A1-6	0.24754	6.24	0.0357	47.1186	Micritic
A1-7	0.0159	6.4727	0.0271	49.8183	Micritic
A1-8	0.034	6.5813	0.095	49.8358	Micritic
A1-9	0.3583	5.3524	0.0746	44.5338	Micritic
A4-1	0.8116	5.8358	0	47.1449	Micritic
A4-2	0.6024	5.1017	0	43.6412	Micritic
A4-3	0.0248	0.0185	0.6479	55.3602	Spar
A4-4	0.009	0.0116	0.4134	55.1553	Spar
A4-5	0	0.0386	0.6675	55.166	Spar
A4-6	0	0.0359	0.776	55.559	Spar
A4-7	0	0.3792	0	55.9506	Spar
A4-8	0.5095	5.6229	0	51.2423	Micritic
A5-1	0.3467	5.1273	0	44.1986	Micritic
A5-2	0.3057	3.9905	0	45.5331	Micritic
A5-3	0.0294	0.1037	1.0066	52.2456	Spar
A5-4	0.009	0.0765	0.6915	51.2728	Spar
A5-5	0.0023	0.0371	0.474	54.106	Spar
A5-6	0.009	0.0423	0.5948	54.689	Spar
A5-7	0	0.0177	0.5176	53.5494	Shell
A5-8	0.0384	0.0149	0.5717	54.1441	Shell
A5-9	0.081	0.0179	1.01	55.4053	Shell
A5-10	0	0.0033	0.2087	55.1102	Shell
A5-11	0.0495	0.0314	1.1087	54.7995	Shell
A5-12	0	0.0335	1.1447	55.4901	Shell
A6-1	0.0293	0	0.4966	55.3165	Spar
A6-2	0.0225	0	0.6892	55.0292	Spar
A6-3	0.0764	0	0.5398	54.5898	Spar
A6-4	0.0157	0	0.628	54.3208	Spar
A6-5	0	0	0.6326	55.5066	Spar
A6-7	0	4.142	0	53.3066	Micritic
A6-8	0.045	0.196	0.9652	56.4666	Spar

Chapter 5: Discussion

5.1 Introduction

The discussion will take properties and characteristics described in Chapter 4 and apply them with current theories of carbonate formation. The discussion will focus on crystal morphology, lime mud neomorphism, popcorn structures, polymictic conglomerate, layering, and erosion.

The absence of an allochemical component or even a biological framework suggests that formation is abiogenic. There may be biological process mediating carbonate precipitation, however precipitation is more likely influenced by non-biological processes. The discussion will therefore be directed towards non-biological processes.

5.2 Layering and Concretionary Formation

Several of the mounds have a poorly defined layering. This signifies non-continuous or periodic formation of the carbonate mounds. Periodic growth resulting in the creation of layers is also observed in concretions (Pratt 2001). For the mounds to truly be concretionary formations, concentric internal layering and a bioclastic nucleus needs to be present. Concentric layers and a bioclastic nucleus (or component) were not identified on any of the samples, suggesting growth is not analogous with concretions.

Myers (1974) discusses microscale zoning in drusy sparry calcite to be a result of subtle variations in trace elements of the pore water. The zoning records crystal growth histories and changes in pore water chemistry over time. Chemical analyses on crystal composition were not accurate, and therefore microscale chemical zoning can not be fully discussed.

5.3 Crystal Morphology and Mineralogy

Folk (1974) defines the relationship of fluid Mg/Ca ratios and the resultant crystal morphology, composition and carbonate mineralogy in abiotic carbonates to have meteoric fluids produce equant low-magnesium calcite and to have marine fluids produce acicular high-magnesium calcite. The crystal morphology in the carbonate samples can be summarized into two forms: (1) microcrystalline low-magnesium micrite and (2) bladed, radial or acicular low-magnesium sparite. The cryptocrystalline low-magnesium calcite identified in samples suggests meteoric pore water. The acicular, banded and unbanded, sparite with low-magnesium is not discussed in Folk's (1974) regime.

Given and Wilkinson (1985) outline a more encompassing relationship between crystal morphology and the ambient depositional fluid. Crystal morphology may be linked with the saturation levels of the fluid and the resultant crystal growth rates. Given and Wilkinson have (1985) documented acicular low magnesium calcite occurring in meteoric-vadose settings. Similarly, it has been documented that high-magnesium equant calcite occurs in shallow marine deposits. Given and Wilkinson (1985) attributed crystal morphology to be associated with the degree of carbonate saturation and rates of fluid flow. Acicular calcite may predominate in higher saturation and fluid flow settings. Equant calcite may predominate in lower saturation and fluid flow settings.

The crystal morphology of the carbonate samples is not a good indicator for the nature of the fluid flow. A diverse spectrum of crystal forms associated with varying pore water environments, with different levels of ambient Mg/Ca ratios, has been cited in the literature.

It may be considered that the samples has been re-deposited on the sea floor as a type of clast. This hypothesis means that they are not *in situ* deposits. Morphological variation in the six specimens would have to be interpreted as a result of erosional processes. The extensive popcorn structures that were observed on samples A1 and A3 are unlikely to be erosional.

5.4 Lime Mud Neomorphism (Diagenesis)

The absence of an internal framework, the absence of an identifiable allochemical component, and the massive nature of the microspar suggests that some degree of diagenesis has occurred and that the micrite may be neomporhic.

Tucker and Wright (1990) propose that modern lime muds have a variable mineralogy, depending on the portion attributed to the breakdown of green algae (aragonite formation), red algae (calcite formation), coccoliths – planktonic foraminifera (calcite, low Mg) and abiogenic precipitation (aragonite, calcite high Mg). These components are not distinguishable in many ancient limestones that are composed of equant micrite crystals ($2\mu\text{m}$ to $3\mu\text{m}$ in size), a similar composition with the lime mud samples in this study.

Crystal neomorphism, either attributed from early meteoric diagenesis or burial diagenesis, results in the formation of microspar ($5\mu\text{m}$ to $10\mu\text{m}$) to pseudospar ($> 30\mu\text{m}$) crystals from the original precipitated fabric. Lasemi and Sandberg (1984) stated that neomorphic crystals, or neomorphic spar, form from the dissolution of some grains and the syntaxial overgrowth of others. Neomorphic spar has four distinguishable properties

in thin section: (1) irregular crystal boundaries, (2) irregular crystal size distribution, (3) gradational boundaries, and (4) the presence of floating grains.

The micrite portions in the carbonate samples in this study have many parallels with neomorphic spar. The micrite-grade regions have irregular and many times unidentifiable crystal boundaries. No gradation on a microscale can be identified, however the large zones of light brown micrite may be attributed to a gradationally boundary between sparite and micrite crystals. There are also numerous quartz grains floating in the micrite. With this in mind, the expected level of neomorphic spar in the samples should be relatively low. Although the full processes of neomorphism are not fully understood, Tucker and Wright (1990) conclude the neomorphism is inhibited with increasing percentages of clay in the limestone. Regardless, the micrite crystals in the carbonate samples have many similarities with neomorphic spar.

5.5 Polymictic Conglomerate

The polymictic conglomerate found in some of the samples suggest that recent (< 12Ka) precipitation has occurred. The nature of the material, various siliciclasts of various sizes, is very similar to what would be found in glaciomarine deposits. The clasts can be then interpreted as intraclasts of local glacial deposits. It can also be inferred that a brecciation of the carbonate mounds would have occurred before cementation of the polymictic conglomerate because of the presence of lime mud clasts within the conglomerate. The origin of the cementation of the polymictic conglomerate has not been defined, but it may be associated the process that brecciated the carbonate mound. Some

sparite has formed so late in the life of the samples that it could be assumed to be a chemical precipitate.

5.6 Popcorn Structures

The popcorn structures on the carbonate samples have been termed 'popcorn' because of their similar morphological shape to cave popcorns. Internally they differ, the cave popcorns are concentrically laminated and the mound popcorns do not have any lamination. Thraillkill (1976) outlines a combination of processes that contribute to cave popcorn formation, such as seepage, surface flow, drip water splash, capillary action or condensation.

Popcorns look like expansion from within the structures, signifying that fluid seepage may be the formation mechanism of the popcorns. The presence of organics within the popcorns could mean that seeping hydrocarbons are the mediating mechanism. Hydrocarbons could be seeping out of faulted zones (although none are known in the region to date) or from underlining Palaeozoic deposits (i.e. coal). Hydrocarbon presence results in carbonate precipitation through bacterial reduction and alteration in ambient fluid geochemistry (Stake *et al.*, 1999).

The fact that not all samples have the popcorn structures may be related to the depth of where the mound occurs. The mounds are located on a ridge, and those mounds occurring in deeper waters (or shallower waters) may have a more extensive exposure to fluid seepage (or other mechanisms).

5.7 Erosion

The large irregular pores found in the carbonate samples could be classified as channel pores according to classification scheme of Choquette and Pray (1970). A pore of this nature is typically a dissolution feature that occurs in unsaturated waters.

The smaller pores have a more regulated structure and are probably bioerosion, or otherwise termed bores. The pores have a regulated structure, size (few millimetres) and length, which are all characteristics of bores (Choquette and Pray, 1970). Identification of the boring organism has not been concluded. It can be proposed that boring may be caused by arctic boring clams or sponges, the most common boring organisms in the area of origin. It should be considered that these small pores may be related to other structures, such as gas venting.

5.8 Origin

Table 5.1 summarizes the interpretation of each feature documented with the studied samples and notes on which type of specimen, eroded, layered or popcorn, the feature occurs.

Table 5.1: Interpretation of documented features of each sample studied.

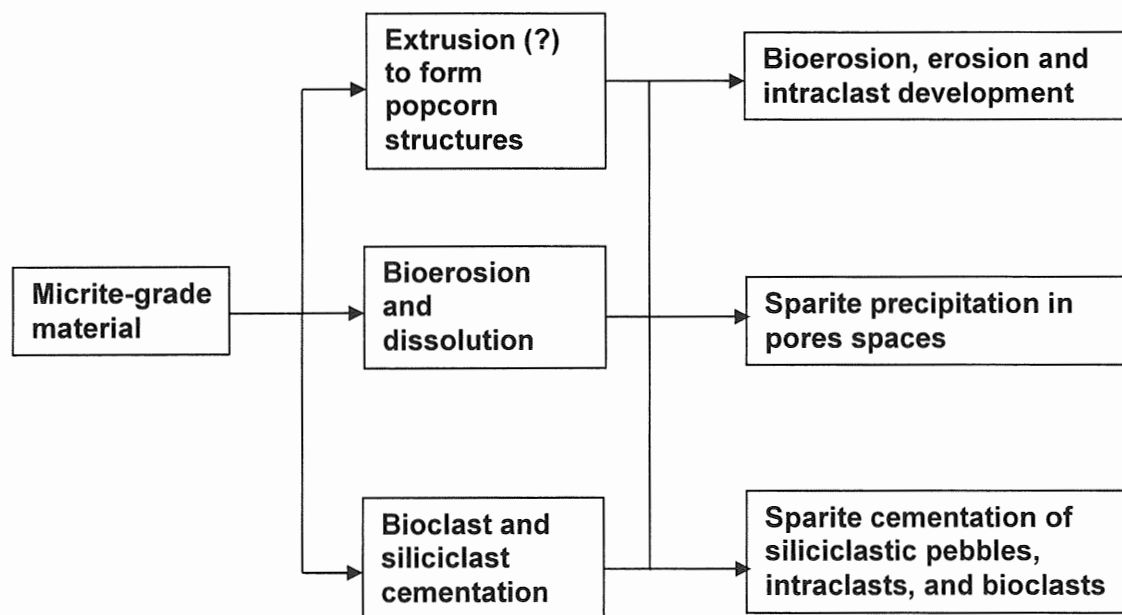
Surficial Textures	Interpretation	Popcorn	Layered	Eroded
Layering	Periodic Growth		X	X
Popcorns	Extrusions	X		
Erosion	Bioerosion and dissolution	X	X	X
Bioclasts	Biological Activity	X	X	X
Siliciclastic Clasts	Recent Precipitation	X		

By providing an interpretation for each feature, it implies that each feature may result from a separate process and therefore numerous processes have contributed to the formation of these carbonate structures. However, if it is considered that all features are the result of a single mechanism the formation of the carbonate mounds is most likely associated by the seepage of a hydrocarbon or methane rich fluid. All features observed in the studied samples can also be observed in other carbonates formed from fluid seepage. The most diagnostic feature is the expansion or extrusion popcorn structures, which may have formed as fluid exhumed through the mounds.

5.9 Timing

Figure 5.1 is a summation of the formation sequence of individual features or processes that contributed to the studied specimens.

Figure 5.1: Formation sequence of features and processes associated with the studied carbonate specimens.



It must be concluded that the micrite-grade material, or lime mud, is the first feature to originate because all other features emanate from the micrite-grade body of the mound. The next sequence of events would be the expansion of fluids to form the popcorns structures, a series of boring erosion and chemical dissolution, and cementation of bioclasts and siliciclasts on the surface to form the agglutinated texture. The final sequence of events that can be recognized is more erosion, which may have resulted in the formation of intraclasts, and sparite formation in the pores and as a cement.

Chapter 6: Conclusions

6.1 Timing

The formation of micrite-grade parts would have been the first event to occur. Boring may have occurred after this time, based on the fact that some are infilled with sediment. All events involving sparite precipitation must then be considered synchronous because no evidence indicates separate sparite forming events.

6.2 Possible Origin

The characterization of the samples in this study has not yet produced sufficient data from which an origin can be inferred. As discussed in Chapter 5, current data indicate that the mounds may originate from bacterial reduction of hydrocarbon seeps, seawater geochemistry at the sediment interface, diagenesis of a modern type lime mud, or the circulation of various pore water fluids. The biological component is not discussed, however it should be noted that the origin may be related to biological activity (sediment surface stirring, microbial reduction) or the degradation of carbonate clasts (shells).

6.3 Classification

The fragments are mud dominant, with little to no allochemical component and little to no internal structure. The origin of the mound is therefore undetermined. With the present data the suitable classification is a shallow marine carbonate mud mound.

6.3 Future Work

A detailed study of the local bathymetry, sediment type, and bedrock geology in the area of distribution would assist in further characterizations. Further sample collection would also help determine representative features, so that a more detailed and focused analysis could be performed. Finally, a comparative study with other structures would assist in identifying the process that formed the mounds.

Isotope chemistry would strongly aid in identifying the origin of the mounds. A continued analysis of sparite and micrite crystal morphology and its relationship with fluid chemistry would also help determine the origin of the mounds.

References

- Bosence, D.W. J. and Bridges, P.H. 1995. A review of the origin and evolution of carbonate mud-mounds. Special Publication on the International Association of Sedimentologists, 23: 1-9.
- Chafetz, H.S. and Folk, R.L. 1984. Travertines, depositional morphology and the bacterially constructed constituents, *Journal of Sedimentary Petrography*, 54: 289-316.
- Choquette, P.W. and Pray, L.C. 1970. Geologic nomenclature and classification of porosity in sedimentary carbonates. *American Association of Petrol. and Geol. Bulletin*, 54: 207-250.
- Curtis, C.D. and Coleman, M.L. 1986. Controls on the precipitation of early diagenetic calcite, dolomite, and siderite concretions in complex depositional sequences. In: D.L. Gautier (ed.), *Roles of Organic Matter in Sediment Diagenesis*. SEPM Special Publication, 38: 23-33.
- Demico, R.V. and Hardie, L.A. 1994. Sedimentary structures and early diagenetic features of shallow marine carbonates, *SPEM Atlas series 1*, 177-179.
- Dunham, R.J. 1962. Classification of carbonate rocks according to depositional texture. In W.E. Ham (ed.), *Classification of Carbonate Rocks*, American Association of Petroleum Geologists Memoir 1: 108-121.
- Embry, A.F. and Klovan, J.E. 1971. A Late Devonian reef tract on Northeastern Banks Island, N. W. T. *Bulletin of Canadian Petroleum Geology*, 19: 4.
- Folk, R.L. 1974. The natural history of crystalline calcium carbonate: effects of magnesium content and salinity. *Journal of Sedimentary Petrology*, 44: 40-53.
- Folk, R.L. 1962. Spectual Subdivision of Limestone Types. In W.E. Ham (ed.), *Classification of Carbonate Rocks*, American Association of Petroleum Geologists Memoir 1: 62-82.
- Folk, R.L. 1959. Practical petrographic classification of limestones. *American Association of Petroleum Geologists Bulletin*, 43: 1-38.

Given, Kevin R. and Wilkinson, B.H. 1985. Kinetic control of morphology, composition, and mineralogy of abiotic sedimentary carbonates. *Journal of Sedimentary Petrology*, 55: 100-118.

James, N.P. and Bourque, P.A. 1992. Reefs and mounds. In: R.G. Walker and N.P. James (ed.), *Facies Models: Response to Sea Level Change*, Geological Association of Canada, *Geotext* vol. 1: 323-347.

Josenhans, H. and Lehman, S. 1999. Late glacial stratigraphy and history of the Gulf of St. Lawrence, Canada. *Canadian Journal of Earth Science*, 36: 1327-1345.

Josenhans, H., Zevenhuizen, J. and MacLean, B. 1990. Preliminary seismostratigraphic interpretations from the Gulf of St. Lawrence. In *Current Research, Part B*, Geological Survey of Canada, Paper 90-1B: 59-75.

Lasemi, Z. and Sandberg, P.A. (1984) Transformation of aragonite-dominated lime muds to microcrystalline limestones. *Geology*, 12: 420-423.

Meyers, W.J. 1974. Carbonate cement stratigraphy of the Lake Valley Formation (Mississippian), Sacramento Mountains, New Mexico. *Journal of Sedimentary Petrology*, 44: 837-861.

Mozley, P.S. 1996. The internal structure of carbonate concretions in mudrocks: a critical evaluation of the conventional concentric model of concretion growth. *Sedimentary Geology*, 103: 85-91.

Pratt, B.R. 2001. Septarian concretions: internal cracking caused by synsedimentary earthquakes. *Sedimentology*, 48: 189-213.

Riding, R. 2002. Structure and composition of organic reefs and carbonate mud mounds: concepts and categories. *Earth-Science Reviews*, 58, 1-2: 163-231.

Stakes, D. S., Orange, D., Paduan, J.B., Salamy, K.A., and Maher, N. 1999. Cold-seeps and authigenic carbonate formation in Monterey Bay, California. *Marine Geology*, 159: 93-109.

Steinen, R.P. 1978. On the diagenesis of lime mud: scanning electron microscope observations of subsurface material from Barbados. *WI. J. sedim. Petrol.*, 45: 1139-1147

Thrailkill, J., 1976. Speleothems, in Walter, M.R. (ed.) *Stromatolites, Developments in Sedimentology*, 20: 73-86.

Wood, R. 2001. Are reefs and mud mounds really so different? *Sedimentary Geology*, 145, 3-4: 161-171.

Appendix A: Microprobe Photos of the Sampled Areas

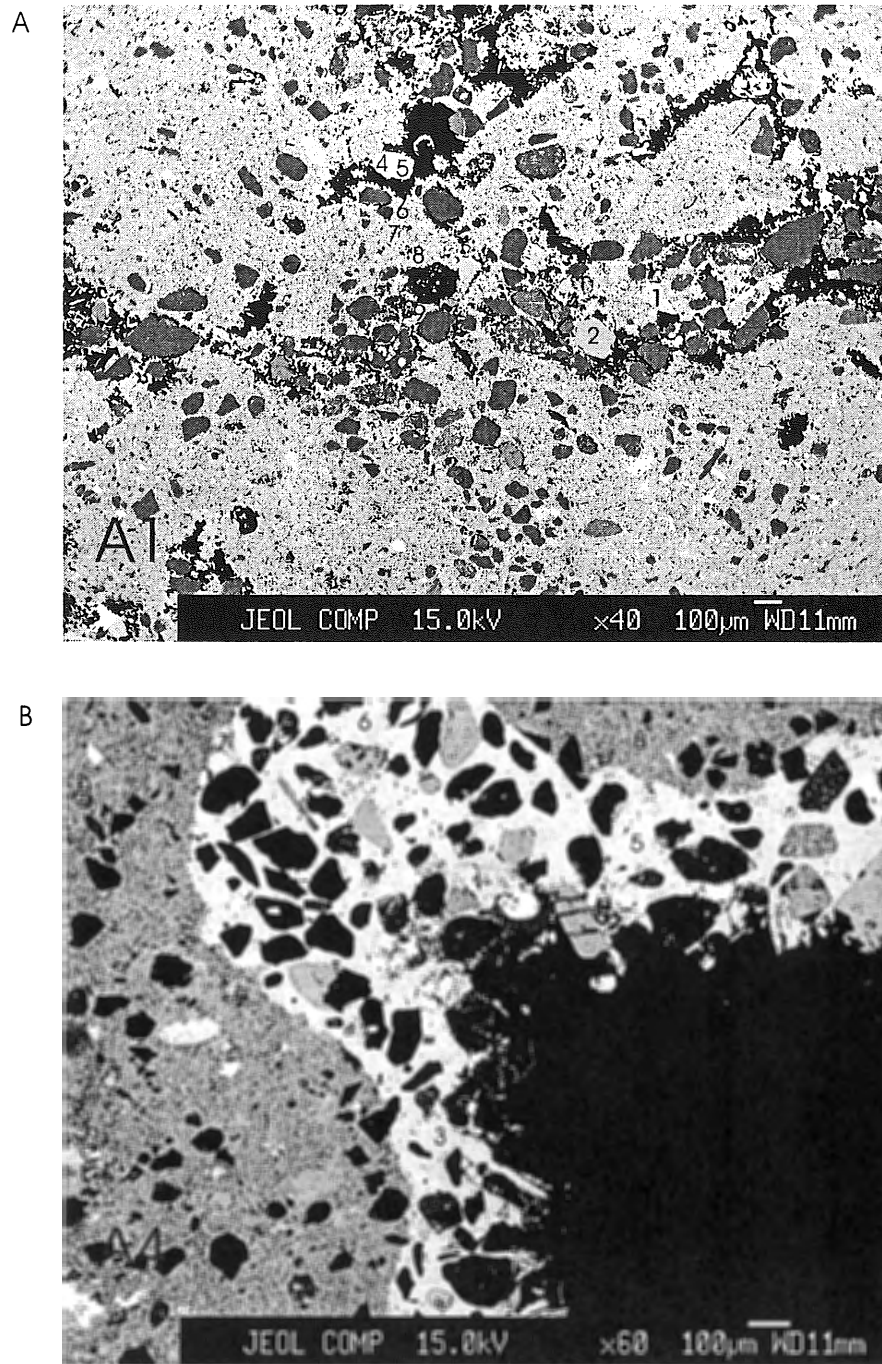


Figure A.1: Sections analyzed in samples A1 and A4 in the microprobe analysis. Areas tested are numbered and can be referenced with Table 4.2 or Appendix B. (A) Micrite matrix and grain composition were analyzed in sample A1. (B) Micrite matrix and sparrite cement were analyzed in sample A4.

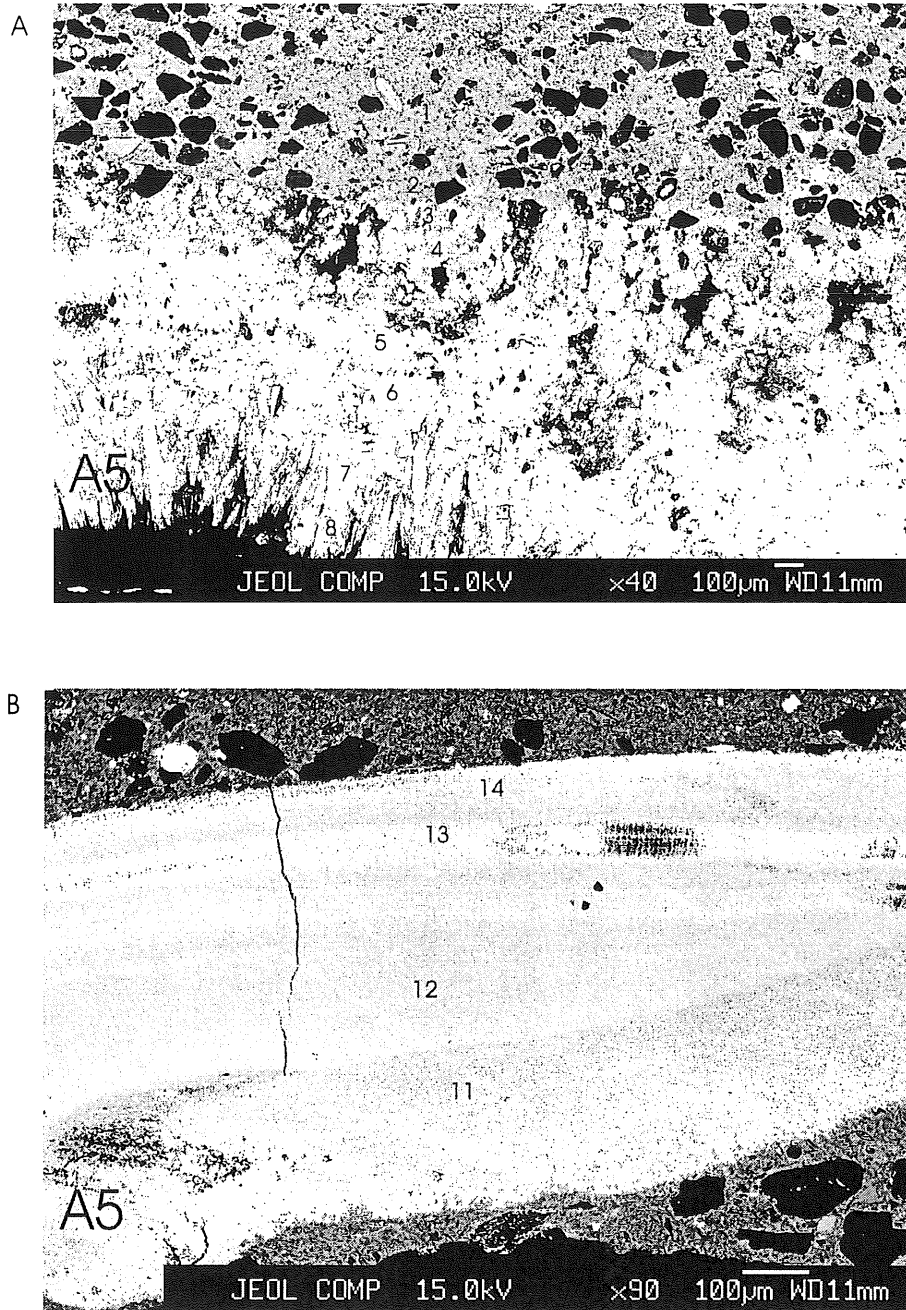


Figure A.2: Sections analyzed from sample A5 in the microprobe analysis. Areas tested are numbered and can be referenced in Table 4.2 or Appendix B. (A) A series of 9 tests were taken through a progression of micrite sparite. (B) A series of 5 tests were taken from a shell in sample A5, so a chemical comparison could be made with sparite and micrite carbonates.

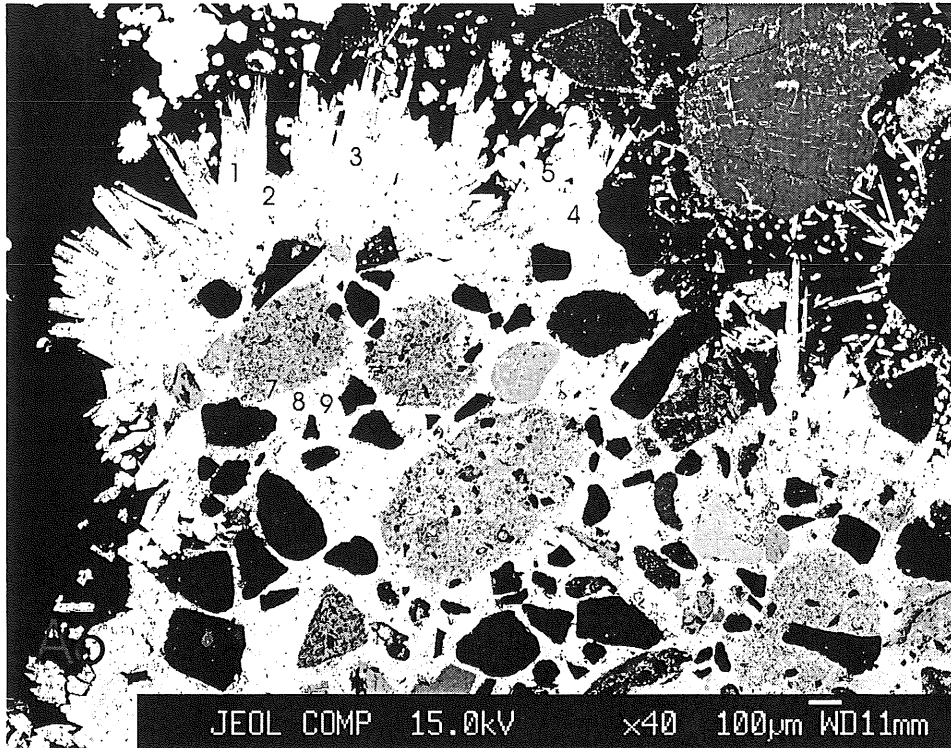


Figure A.3: Sections analyzed from sample A6 in the microprobe analysis. Spots tested are numbered and can be referenced in Table 4.2 or Appendix B. Sparite cement was primarily analyzed in sample 6.

Appendix B: Complete Results of Microprobe Analysis

	Sample A1-1	Sample A1-2	Sample A1-3	Sample A1-4
FeO	0.0455	0.0637	0.0386	0.0409
CaO	0.0643	0.1618	5.2808	56.6928
MgO	0.0012	0	0	0.084
SiO ₂	64.903	67.1225	62.1366	0
BaO	0.3349	0.1421	0.335	0.54
MnO	0	0.0068	0	0.0182
SrO	0	0	0.1194	0
Na ₂ O	0.2368	3.2129	8.7432	0
Al ₂ O ₃	17.1496	17.959	22.8272	0

	Sample A1-5	Sample A1-6	Sample A1-7	Sample A1-8
FeO	0.0522	0.2475	0.0159	0.034
CaO	52.1674	47.1186	49.8183	49.8358
MgO	4.5432	6.24	6.4727	6.5813
SiO ₂	0	2.3787	0	0
BaO	0.0268	0.0133	0.0089	0.0022
MnO	0	0.0204	0	0.034
SrO	0.0571	0.0357	0.0271	0.095
Na ₂ O	0.0716	0.1399	0.1434	0.1591
Al ₂ O ₃	0	0.9387	0	0

	Sample A1-9	Sample A4-1	Sample A4-2	Sample A4-3
FeO	0.3583	0.8116	0.6024	0.0248
CaO	44.5338	47.1449	43.6412	55.3602
MgO	5.3524	5.8358	5.1017	0.0185
SiO ₂	3.3278	0.8432	3.7927	0
BaO	0.0421	0.0508	0.0132	0.0245
MnO	0	0	0	0
SrO	0.0746	0	0	0.6479
Na ₂ O	0.1909	0.1673	0.1619	0.4025
Al ₂ O ₃	1.1225	0.6271	1.3989	0

	Sample A4-4	Sample A4-5	Sample A4-6	Sample A4-7
FeO	0.009	0	0	0
CaO	55.1553	55.166	55.599	55.9506
MgO	0.0116	0.0386	0.0359	0.3792
SiO ₂	0	0	0	0
BaO	0.0379	0	0.0223	0.0536
MnO	0.0226	0	0.0023	0.1039
SrO	0.4134	0.6675	0.7766	0
Na ₂ O	0.2108	0.4765	0.4686	0.025
Al ₂ O ₃	0	0	0.0086	0.0086

	Sample A4-8	Sample A5-1	Sample A5-2	Sample A5-3
FeO	0.5	0.3467	0.3057	0.0294
CaO	51.2423	44.1986	45.5331	52.2456
MgO	5.6229	5.1273	3.9905	0.01037
SiO ₂	0	5.0964	3.1851	0
BaO	0.0509	0.0066	0.0199	0.0112
MnO	0	0.0068	0.0136	0
SrO	0	0	0	1.006
Na ₂ O	0.204	0.217	0.2442	0.4266
Al ₂ O ₃	0.1656	1.8449	1.9617	0.0067

	Sample A5-4	Sample A5-5	Sample A5-6	Sample A5-7
FeO	0.009	0.0023	0.009	0
CaO	512728	54.106	54.689	53.5494
MgO	0.0765	0.0371	0.0423	0.0177
SiO ₂	0	0	0	0
BaO	0.0157	0.0492	0.0179	0
MnO	0	0	0	0
SrO	0.6915	0.474	0.5948	0.5176
Na ₂ O	0.4253	0.3902	0.4314	0.2888
Al ₂ O ₃	0	0	0.0016	0.0045

	Sample A5-8	Sample A5-9	Sample A5-10	Sample A5-11
FeO	0.0384	0.018	0	0.0495
CaO	54.1441	55.4053	55.1102	54.7995
MgO	0.0149	0.0179	0.0033	0.0314
SiO ₂	0	0	0	0
BaO	0.0112	0	0	0
MnO	0	0	0.0587	0.0406
SrO	0.5717	1.01	0.2087	1.1087
Na ₂ O	0.3586	4899	0.5041	0.4613
Al ₂ O ₃	0	0.0156	0.0029	0.0115

	Sample A5-12	Sample A6-1	Sample A6-2	Sample A6-3
FeO	0	0.0293	0.0225	0.0764
CaO	55.4901	55.3165	55.0292	54.5898
MgO	0.0335	0	0	0
SiO ₂	0	0	0	0
BaO	0	0.0601	0.0156	0.0267
MnO	0.0158	0.018	0	0.009
SrO	1.1447	0.4966	0.6892	0.5398
Na ₂ O	0.458	0.4139	0.3255	0.4697
Al ₂ O ₃	0.014	0.0089	0	0

	Sample A6-4	Sample A6-5	Sample A6-6	Sample A6-7
FeO	0.0157	0	0.7023	0
CaO	54.3208	55.5066	47.4093	53.3066
MgO	0	0	0.4319	4.142
SiO₂	0	0	4.2295	0
BaO	0.0511	0.04	0.0857	0
MnO	0	0	0	0
SrO	0.628	0.6326	0.7241	0
Na₂O	0.4151	0.3482	0.4477	0.2627
Al₂O₃	0	0	2.1956	0

	Sample A6-8	Sample A6-9
FeO	0.045	0.0382
CaO	56.4666	39.3871
MgO	0.0196	0.0447
SiO₂	0	0
BaO	0.0534	0.0955
MnO	0.0338	0
SrO	0.9652	0.8103
Na₂O	0.5473	0.5959
Al₂O₃	0	0